

# Quantum Computing Quantum Monte Carlo

Yukun Zhang,<sup>1,2,\*</sup> Yifei Huang,<sup>3,\*</sup> Jinzhao Sun,<sup>4,5</sup> Dingshun Lv,<sup>3</sup> and Xiao Yuan<sup>1,2,†</sup>

<sup>1</sup>*Center on Frontiers of Computing Studies, Peking University, Beijing 100871, China*

<sup>2</sup>*School of Computer Science, Peking University, Beijing 100871, China*

<sup>3</sup>*ByteDance Research, Zhonghang Plaza, No. 43, North 3rd Ring West Road, Haidian District, Beijing, China*

<sup>4</sup>*Clarendon Laboratory, University of Oxford, Parks Road, Oxford OX1 3PU, United Kingdom*

<sup>5</sup>*Quantum Advantage Research, Beijing 100080, China*

Quantum computing and quantum Monte Carlo (QMC) are respectively the state-of-the-art quantum and classical computing methods for understanding many-body quantum systems. Here, we propose a hybrid quantum-classical algorithm that integrates these two methods, inheriting their distinct features in efficient representation and manipulation of quantum states and overcoming their limitations. We first introduce non-stoquasticity indicators (NSIs) and their upper bounds, which measure the sign problem, the most notable limitation of QMC. We show that our algorithm could greatly mitigate the sign problem, which decreases NSIs with the assistance of quantum computing. Meanwhile, the use of quantum Monte Carlo also increases the expressivity of shallow quantum circuits, allowing more accurate computation that is conventionally achievable only with much deeper circuits. We numerically test and verify the method for the  $N_2$  molecule (12 qubits) and the Hubbard model (16 qubits). Our work paves the way to solving practical problems with intermediate-scale and early-fault tolerant quantum computers, with potential applications in chemistry, condensed matter physics, materials, high energy physics, etc.

A critical task in quantum physics is to find eigenstates and eigenenergies of quantum many-body systems for their wide applications in quantum chemistry [1–3], materials [4], condensed matter physics [5], high energy physics [6, 7], etc. Based on different approximations, various classical computational methods have been invented, including perturbation theories [8], variational tensor network approaches [9–11], self-consistent density functional theory or embedding methods [12–16], quantum Monte Carlo (QMC) [17–19], machine learning [20–22], etc. In particular, as one of the state-of-the-art approaches, QMC has drawn great attention and has been widely exploited to study chemistry and condensed matter physics problems, solving problems with up to around 800 electrons [23]. However, since the Hilbert space of quantum systems increases exponentially with the system size, all these classical methods have certain limitations. Specifically, QMC represents quantum states by an effective (realized via Monte Carlo) superposition of classical basis states, it generally suffers from the notorious sign problem [24], prohibiting its usefulness for strongly-correlated systems.

On the other hand, quantum computers can more naturally represent and manipulate quantum states, thus offering the opportunity to overcome the aforementioned challenges [25]. Different quantum algorithms, such as adiabatic state preparation [26], quantum phase estimation [27–29], and the recently proposed/improved methods for ground state energy estimation [30–36], have been proposed to solve the eigenstate problem. Yet, those quantum algorithms generally require a deep quantum circuit that is only achievable with fault-tolerant universal quantum computers. Near-term quantum computers however can only control a limited number of qubits with relatively noisy operations, corresponding to the

noisy intermediate-scale quantum (NISQ) era [37]. While many recent works have shown the potential applicability of quantum computing using NISQ devices [38–41], whether they are sufficiently powerful (large and deep) to solve realistic problems still remains open.

Here we introduce a hybrid approach that integrates QMC and quantum computing, leveraging their complementary strengths in representing and processing quantum states, meanwhile mitigating their respective weaknesses of exponentially small average signs and hardware limitations. We first introduce non-stoquasticity indicators (NSIs) and their upper bounds, measuring the seriousness of the sign problem. Then we consider full configuration interaction quantum Monte Carlo (FCIQMC) [19, 42] and show how to efficiently implement it using a quantum computer. Since the quantum states (walkers) are now prepared with an optimized quantum circuit, the sign problem of FCIQMC is greatly relieved. This has been verified numerically for the  $N_2$  molecule (12 qubits) and the Hubbard model (16 qubits). We show a drastic decrease in NSIs, the energy variance (with a fixed number of walkers), and the number of walkers (to ensure a desired variance) using our method. The results also show much higher accuracies for QC-FCIQMC, which are only achievable with much deeper circuits for conventional quantum computing approaches.

**Background.**— Here we review the basics of QMC and quantum computing. We consider the problem of finding the ground state of Hamiltonian  $H$ . We focus on  $H$  with real matrix elements and refer to Ref. [43] for the general case.

We consider projector QMC, a subclass of QMC, which effectively represents the state as a superposition of walkers (states such as Slater determinants) and realizes the

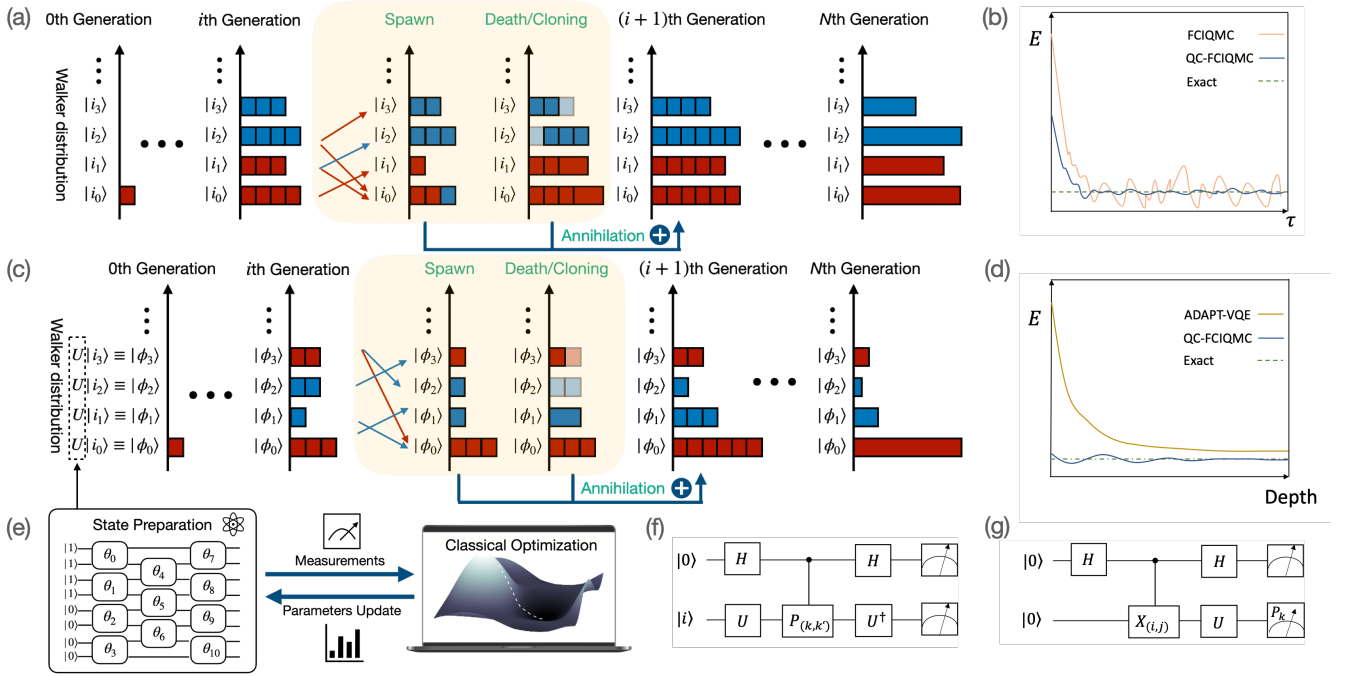


Figure 1. (a) Sketch of the spawning, death/cloning, and annihilation steps in FCIQMC. Red and blue colors represent walkers with positive and negative signs respectively. Red and blue arrows represent the sign of  $H_{ji}$ . The transparent boxes represent dead walkers, while the elongated walkers are the cloned ones. (b) Sign problem comparison for our QC-FCIQMC and FCIQMC. (c) The procedure of QC-FCIQMC. The quantum circuit  $U$  that generates the new basis is obtained from VQAs, such as the one shown in (e). (d) Energy convergence comparison of ADAPT-VQE and QC-FCIQMC. (e) State preparation circuit. (f) Quantum circuit for evaluating  $|H_{ji}|^2$ . (g) Circuit for evaluating the real part of  $H_{ji}$ .

imaginary-time evolution (ITE) of the state by stochastically propagating the walkers. Denote the walkers by  $\{|i\rangle\}$  and the initial state by  $|\psi(0)\rangle = \sum_i c_i(0) |i\rangle$  with coefficients  $c_i(0)$ , projector QMC aims to realize the ITE of the state as  $|\psi(\tau)\rangle \propto e^{-(H-S)\tau} |\psi(0)\rangle$  with  $\tau > 0$  and certain parameter  $S$ . Specifically, for FCIQMC (see Fig. 1(a)), we first generate  $N_i(\tau)$  number of walker  $|i\rangle$  at  $\tau = 0$ ; Then, for small  $\Delta\tau$ , we repeatedly update each walker  $|i\rangle$  through (1) spawning — spawn a child walker  $|j\rangle$  ( $j \neq i$ ) with probability  $|H_{ji}|\Delta\tau$  with the same sign as walker  $|i\rangle$  multiplied by  $-H_{ji}/|H_{ji}|$  ( $H_{ij} = \langle i|H|j\rangle$ ); (2) Death or cloning — the walker  $|i\rangle$  dies with probability  $(H_{ii} - S)\Delta\tau$  (if  $H_{ii} - S > 0$ ) and clones itself with probability  $|(H_{ii} - S)|\Delta\tau$  otherwise; (3) Annihilation — annihilate same walker pairs with opposite signs. While QMC could deterministically find the ground state with large  $\tau$ , it suffers from the sign problem [24]. We shortly show a quantitative measure of the sign problem.

For quantum computing, we consider variational quantum algorithms (VQA) designed for near-term quantum devices (see Fig. 1(e)). Here, we consider variational quantum eigensolver (VQE) [44, 45] as an example. For the Hamiltonian  $H$ , we approximate its ground state as  $|\phi_0(\vec{\theta})\rangle = U(\vec{\theta})|\bar{0}\rangle$  with a parameterized quantum circuit  $U(\vec{\theta})$  and an initial state  $|\bar{0}\rangle$ . Then we apply a classical optimizer to search for parameters  $\vec{\theta}$  that min-

imize the energy  $E(\vec{\theta}) = \langle \phi_0(\vec{\theta}) | H | \phi_0(\vec{\theta}) \rangle$ . While recent works have demonstrated the potential power of variational quantum algorithms [37–41], they still have several limitations. First, due to the short coherence time of near-term quantum devices, the circuit depth is limited, which may be incapable to approximate the desired ground state [46, 47]. Second, the landscape of  $E(\vec{\theta})$  might have many local minima [48], making it hard to converge to the optimal solution. Third, VQE has the barren plateau problem [49–51] and the absence of automatic differentiation also makes efficient optimization challenging.

Shortly, we introduce our hybrid approach that overcomes or mitigates these limitations, see Fig. 1 (b, d).

**Sign problem indicators.**— According to Troyer [24], a necessary condition for the sign problem is non-stoquasticity. Consider a general walker basis (orthonormal states)  $\{|\phi_i\rangle\}$ , a Hamiltonian is called “stoquastic” when all its off-diagonal terms (in the walker basis) are non-positive. For a thermal state  $e^{-\beta H}/Z$  with  $Z = \text{Tr}[e^{-\beta H}]$ , the expectation of observable  $A$  is  $\langle A \rangle = \text{Tr}[Ae^{-\beta H}]/Z$ . Denote  $G = \alpha I - H$  with  $\alpha = \max_i H_{ii}$ ,

and we have

$$\langle A \rangle = \frac{\text{Tr}[Ae^{\beta G}]}{\text{Tr}[e^{\beta G}]} = \frac{\sum_{k=0}^{\infty} \frac{\beta^k}{k!} \sum_{i_0, i_1, \dots, i_k} A_{i_0 i_1} G_{i_1 i_2} \cdots G_{i_k i_0}}{\sum_{k=0}^{\infty} \frac{\beta^k}{k!} \sum_{i_1, i_2, \dots, i_k} G_{i_1 i_2} G_{i_2 i_3} \cdots G_{i_k i_1}}, \quad (1)$$

where we denote  $M_{ij} := \langle \phi_i | M | \phi_j \rangle$  for any operator  $M$ . When  $H$  is stoquastic, every element of  $G$  is positive, and so are the expanded terms of  $\text{Tr}[e^{\beta G}]$ .

On the other hand, when  $H_{ij}$  has positive off-diagonal terms, the expansion has a mixture of signs, leading to the sign problem.

To quantify the sign problem of Hamiltonian  $H$ , we partition it as  $H = H_+ + H_-$  with  $(H_-)_{ij} = H_{ij}$  ( $[i = j]$  or  $[i \neq j \text{ and } H_{ij} < 0]$ ) and  $(H_+)_{ij} = H_{ij}$  [ $i \neq j$  and  $H_{ij} > 0$ ]. The bosonic form [24] of  $H$  is  $\tilde{H} = H_- - H_+$ , which is stoquastic and hence has no sign problem. The non-stoquasticity indicator (NSI) is defined by

$$S(H) = \frac{\text{Tr}[e^{-\beta \tilde{H}}] - \text{Tr}[e^{-\beta H}]}{\text{Tr}[e^{-\beta H}]} \quad (2)$$

Denote  $s$  to be the sign of the expansion of  $\text{Tr}[e^{\beta G}]$  in Eq. (1), then we have  $S(H) = 1/\langle s \rangle - 1$ . The sign problem indicates an exponentially small average sign  $\langle s \rangle = e^{-\beta \Delta f}$  with  $\Delta f$  being the free energy difference between  $H$  and  $\tilde{H}$ . Thus  $S(H)$  also exponentially increases with  $\beta \Delta f$ . However, it is generally hard to evaluate  $\Delta f$ . Here, we provide an upper bound of  $S(H)$  with more explicit dependence on the matrix element of  $H_{\pm}$ .

**Theorem 1.** *The NSI is upper-bounded by*

$$S(H) \leq 2e^{\beta \|(\alpha - H_-)\|_{L_1}} \sinh(\beta \|H_+\|_{L_1}), \quad (3)$$

where  $\|M\|_{L_1} := \sum_{i,j} |M_{ij}|$  for matrix  $M$ .

A stoquastic Hamiltonian has  $H_+ = 0$ , indicating  $S(H) = 0$  and hence no sign problem. In general, a smaller  $\|H_+\|_{L_1}$  also corresponds to a less serious sign problem, which is consistent with recent works [52–55].

Meanwhile, when we focus on the imaginary time evolution of a specific initial state, say  $\phi_0$ , with time  $\tau = \beta/2$ , we can similarly define the NSI as

$$S(H, \phi_0) = \frac{\langle \phi_0 | e^{-\beta \tilde{H}} | \phi_0 \rangle - \langle \phi_0 | e^{-\beta H} | \phi_0 \rangle}{\langle \phi_0 | e^{-\beta H} | \phi_0 \rangle}. \quad (4)$$

Again,  $S(H, \phi_0)$  measures the sign problem and is related to the average sign. We provide an upper bound of  $S(H, \phi_0)$  as a function of  $\phi_0$  and  $H_{\pm}$ .

**Theorem 2.** *The NSI is upper-bounded by*

$$S(H, \phi_0) = \mathcal{O}(\|\Pi_{\perp} H | \phi_0 \rangle\|), \quad (5)$$

where  $\| |v\rangle \| = \sqrt{\langle v | v \rangle}$  and  $\Pi_{\perp} = I - | \phi_0 \rangle \langle \phi_0 |$ .

Here, we have ignored the dependence on other matrix elements of  $H$  and we refer to Ref. [43] for the complete upper bound [56]. We can see that a good initial state that is close to an eigenstate of  $H$  can also alleviate the sign problem.

### QC-FCIQMC.—

We now introduce our hybrid quantum computing (QC)-FCIQMC approach. The basic idea is to replace the classical walker states  $\{|i\rangle\}$  with states  $\{|\phi_i\rangle\}$  prepared by quantum circuits  $|\phi_i\rangle = U|i\rangle$ , as shown in Fig. 1(c). This new basis is orthogonal by construction because  $\langle j | U^{\dagger} U | i \rangle = \delta_{ij}$ . This is equivalent to considering classical walkers  $\{|i\rangle\}$  with a similarity transformed Hamiltonian  $U^{\dagger} H U$ . We may use a quantum computer to find  $U$  that approximately diagonalizes  $H$  [57, 58], where the off-diagonal part  $U^{\dagger} H U$  is suppressed [59]. According to Theorem 2, finding a good initial state that has a non-vanishing overlap with the ground state can help to mitigate the sign problem. As such, we may not even need to approximately diagonalize  $H$ , but instead, find an approximate ground state, a much simpler task that requires even shallower circuits [45, 60–63]. We can apply VQE methods with a shallow circuit and use them to ease the sign problem (see Fig. 1(b)).

Suppose we have already found  $U$  and replaced  $|i\rangle$  with ‘quantum’ walkers  $|\phi_i\rangle = U|i\rangle$ . Now the wavefunction is expanded as  $|\psi(\tau)\rangle = \sum_i \tilde{c}_i(\tau) |\phi_i\rangle$  where the coefficients  $\tilde{c}_i(\tau)$  follow the imaginary time evolution as

$$\frac{d\tilde{c}_i(\tau)}{d\tau} = - \sum_j (H_{ij} - S\delta_{ij}) \tilde{c}_j(\tau), \quad (6)$$

with  $H_{ij} = \langle \phi_i | H | \phi_j \rangle$  and an adjustable energy shift  $S$ . Now, we need to propagate the walkers to effectively realize the imaginary time evolution. Here, a major challenge is how to realize the spawning process, i.e., to propagate walker  $|\phi_i\rangle$  to  $|\phi_j\rangle$  with probability  $|H_{ji}| \Delta\tau$ . In conventional FCIQMC, this is possible since there is only a known polynomial number of nonzero  $H_{ji}$  for (classical) walkers  $\{|i\rangle\}$ . However, for (quantum) walkers  $|\phi_i\rangle$ , we have no information on the indices that give nonzero  $H_{ji}$ , so naively, we may need to measure all  $H_{ji}$  to realize the spawning process, which is formidable.

Here we introduce an efficient way to realize the spawning process. To evaluate the probability  $|H_{ji}| \Delta\tau$ , we note that  $|H_{ji}|^2 = \langle i | U^{\dagger} H U \Pi_j U^{\dagger} H U | i \rangle$  with  $\Pi_j = |j\rangle \langle j|$ . Suppose the Hamiltonian is expanded as  $H = \sum_k h_k P_k$  with coefficients  $h_k$  and Pauli operators  $P_k$ , then  $|H_{ji}|^2 = \sum_{kk'} h_k h_{k'} p_{kk'}^i(j)$  with  $p_{kk'}^i(j) = \text{Re} \langle i | U^{\dagger} P_k U \Pi_j U^{\dagger} P_{k'} U | i \rangle$  satisfying  $\sum_j |p_{kk'}^i(j)| \leq 1$ . For fixed  $i, k, k'$ , we can use the quantum circuit in Fig. 1(f) to measure  $p_{kk'}^i(j)$  for all  $j$  and hence obtain  $|H_{ji}|$  up to a desired accuracy. We usually get a small number of non-negligible  $|H_{ji}|$ . Then we can apply the quantum circuit in Fig. 1(g) to further estimate the sign

(phase) of  $H_{ji}$ . Note that the quantum circuits for estimating  $|H_{ji}|$  and its sign only introduce one ancillary qubit and at most doubles the unitary  $U$  (apart from a few gates independent of  $U$ ). Meanwhile,  $H_{ji}$  only needs to be measured once and information could be re-used.

We can also efficiently estimate each  $H_{ii}$  using the same quantum circuit and hence realize the death or cloning step. The last annihilation step does not need the quantum computer. After implementing the evolution (with initial walkers  $\phi_0$ ), we can get the energy by the mixed energy evaluation  $E(\tau) = E_0 + \sum_{i \neq 0} \langle \phi_i | H | \phi_0 \rangle \frac{\text{sign}(i)N_i(\tau)}{N_0(\tau)}$ , where  $E_0 = \langle \phi_0 | H | \phi_0 \rangle$ , and  $N_i(\tau)$  and  $\text{sign}(i)$  are the number and sign of walker  $\phi_i$ , respectively. Suppose  $\phi_0$  is obtained by running VQE, then our method effectively introduces corrections from all other  $\phi_i$  by implementing QMC. We summarize the workflow in Fig. 1(c) and Algorithm 1. We used VQE in the algorithm as an example, but it works for general VQAs.

---

### Algorithm 1 QC-FCIQMC

---

**Input:** Hamiltonian  $H$ , total evolution time  $T$ , time step  $\Delta\tau$ .

**Output:** Ground state energy estimation.

Run VQE to determine  $U$  and hence  $\{|\phi_i\rangle = U|i\rangle\}$ .

Generate  $N_0$  walkers  $|\phi_0\rangle$  and let walker set  $\mathcal{D} = \{0\}$ .

**for**  $n$  in range( $T/\Delta\tau$ ) **do**

**for**  $i$  in  $\mathcal{D}$  **do**

    Estimate  $|H_{ji}|$  using the circuits in Fig. 1(f) [64].

**for**  $j$  with nonzero  $|H_{ji}|$  **do**   ▷ **Spawning step**

      For each walker  $|\phi_i\rangle$ , spawn a new walker  $|\phi_j\rangle$  with probability  $\Delta\tau|H_{ji}|$ .

**if** New walker  $|\phi_j\rangle$  spawned **then**

        Estimate  $H_{ji}/|H_{ji}|$  using the circuit in Fig. 1(g)

        Label the new walker  $|\phi_j\rangle$  with the sign of  $|\phi_i\rangle$  multiplied by  $-H_{ji}/|H_{ji}|$ .

        Add  $j$  to  $\mathcal{D}$ .

    Estimate  $p_i = \Delta\tau(H_{ii} - S)$

**if**  $p_i < 0$  **then**   ▷ **Death/cloning step**

      Clone each walker  $|\phi_i\rangle$  with probability  $|p_i|$ .

**else**

      Kill each walker  $|\phi_i\rangle$  with probability  $p_i$ .

**for**  $i$  in  $\mathcal{D}$  **do**   ▷ **Annihilation step**

      Annihilate the walkers  $|\phi_i\rangle$  with opposite signs.

Output the mixed energy.

---

**Numerics.**— Now we present numerical tests of the method. We consider two strongly correlated systems, the  $N_2$  molecule and the Hubbard model, and compare QC-FCIQMC to ADAPT-VQE [45, 60–63] and FCIQMC with single determinant walkers.

For  $N_2$ , we freeze the 1s and 2s orbitals and run ADAPT-VQE with 12 qubits. The walker basis of QC-FCIQMC is prepared by ADAPT-VQE circuits using 12 fermionic operators. We set 10000 walkers to be the threshold for FCIQMC and QC-FCIQMC to start the energy shift procedure. In Fig. 2(a,b), we plot the potential energy surface and the energy difference (devi-

ation) [65] respectively. We see that QC-FCIQMC is able to push the results of shallow circuits to the level of chemical accuracy across all bond lengths, much better than ADAPT-VQE and FCIQMC. Meanwhile, the standard deviation of QC-FCIQMC is much smaller than that of FCIQMC. Therefore, QC-FCIQMC would require a smaller evolution time and fewer energy evaluations to obtain a precise energy estimation.

Next, we consider how circuit depth (the number of operators added in ADAPT-VQE) affects our method. We focus on  $N_2$  at bond length 4.0Å. We plot the effects of energy accuracy improvement and energy variance reduction with an increasing circuit depth in Fig. 2(c). The standard deviation is reduced by two orders from a single determinant basis (FCIQMC) to ADAPT-VQE with 24 operators (QC-FCIQMC). At this depth, QC-FCIQMC achieves the (pessimistically evaluated) standard deviation within the chemical accuracy using only 10000 walkers. Meanwhile, QC-FCIQMC also visibly outperforms ADAPT-VQE for all circuit depths. As shown in Fig. 2(d), the NSI upper bound decreases with increasing circuit depths, in accordance with the theoretical prediction. In Ref. [43], we also show that the total number of walkers needed to ensure a fixed level of variance decreases with the circuit depth. Furthermore, we introduce sampling noise to the spawning process. For each walker  $i$ , we

sample a certain number of  $js$  according to the Hamiltonian magnitude. In Ref. [43], we run QC-FCIQMC for different sample sizes and observe a consistent decrease of bias from the FCI result with increasing sample sizes.

We also test our QC-FCIQMC algorithm on the Hubbard model. Here we choose the Hubbard model of size 2 at half-filling, which requires 16 qubits, and pick  $U/t = 4$ , which exhibits competition between onsite repulsion and hopping effects. In Fig. 2(e, f), we plot the energy fluctuations and walker distributions that manifest the sign problem for single determinant FCIQMC and QC-FCIQMC with 15 layers of Hamiltonian variational ansatz (HV ansatz) [66–68]. One can see that our QC-FCIQMC proposal significantly eases the influence of the sign problem. The fluctuation of the QC-FCIQMC energies is much smaller and the walker population is much more concentrated. In Ref. [43], we also test the systematic energy variance reduction with an increasing number of HV ansatz layers.

**Discussion & Conclusion.**— In this work, we propose a hybrid QC-QMC method. We derive upper bounds to NSIs, which guide the discovery and testing of the effectiveness of the method. The QC-FCIQMC algorithm also relies on a nontrivial efficient realization of the spawning process, which otherwise requires exponential resources. We benchmark the algorithm for  $N_2$  and the Hubbard model, and the results show notable improvements over the single use of QC or FCIQMC.



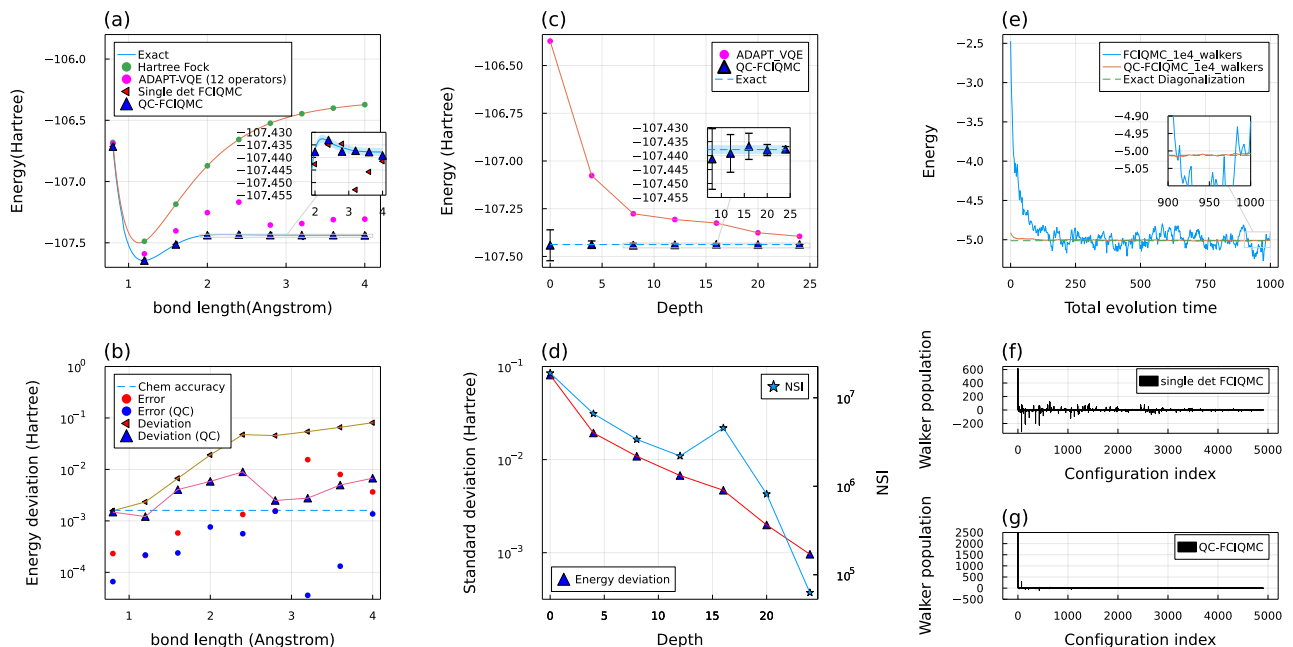


Figure 2. Numerical results of QC-FCIQMC. (a) Potential energy surface for the nitrogen molecule with different methods under the STO-3g basis set. (b) The standard deviation of energy evaluations along the QMC evolution. Here the new walker space of QC-FCIQMC is prepared with circuits from ADAPT-VQE (adding 12 fermionic operators for all bond length). (c) ADAPT-VQE energies and QC-FCIQMC energies with standard deviations for different depths of ADAPT-VQE. (d) Standard deviations from (c) as well as the non-stoquastic indicator with  $\beta = 10^{-1}$ . (e) Comparison of energy fluctuation for FCIQMC and QC-FCIQMC for the Hubbard model. (f) Walker population obtained from single determinant FCIQMC. (g) Walker population from QC-FCIQMC. All numerical simulations in this figure are performed with the original QC-FCIQMC, without sampling approximation.

There are several interesting future directions. First, the derived bounds for NSIs could be exploited to find other basis rotations as a classical means to mitigate the sign problem. Next, our algorithm is compatible with current and near-term quantum hardware, and therefore its detailed resource analysis, error mitigation, and experimental realization also deserve future work. One could also explore the use of the VQE basis and our circuit construction for the deterministic selected-CI variants of FCIQMC [69–72].

Finally, we remark that our method is distinct from other recent QC-QMC proposals [73–77], such as introducing quantum trial states in auxiliary field QMC [74] (AFQMC) method, as well as works from classical QMC literature investigating different choices of walker basis and trial states [78–80]. Regarding the AFQMC work [74], their motivation is to find better trial states in AFQMC method seeks to unbiased the result, while our idea is mitigating the sign problem by replacing the walker basis. Compared to these classical algorithms [73, 75–77], we introduce quantum-circuit-prepared wave functions that are more expressive. Besides, we also provide guarantees regarding the sample complexity of our method in Ref. [43].

*Acknowledgments.*—The authors thank William Huggins

and Sam McArdle for helpful discussions on the sampling procedure, Runze Chi, Tonghuan Jiang, and Ji Chen regarding the Hubbard model and QMC methods. This work is supported by the National Natural Science Foundation of China Grant No. 12175003.

\* These two authors contributed equally to this work.

† xiaoyuan@pku.edu.cn

- [1] G. K.-L. Chan and S. Sharma, Annual review of physical chemistry **62**, 465 (2011).
- [2] S. McArdle, S. Endo, A. Aspuru-Guzik, S. C. Benjamin, and X. Yuan, Reviews of Modern Physics **92**, 015003 (2020).
- [3] Y. Cao, J. Romero, J. P. Olson, M. Degroote, P. D. Johnson, M. Kieferová, I. D. Kivlichan, T. Menke, B. Peropadre, N. P. Sawaya, *et al.*, Chemical reviews **119**, 10856 (2019).
- [4] B. Bauer, S. Bravyi, M. Motta, and G. K.-L. Chan, Chemical Reviews **120**, 12685 (2020).
- [5] B.-X. Zheng, C.-M. Chung, P. Corboz, G. Ehlers, M.-P. Qin, R. M. Noack, H. Shi, S. R. White, S. Zhang, and G. K.-L. Chan, Science **358**, 1155 (2017).
- [6] S. P. Jordan, K. S. M. Lee, and J. Preskill, Science **336**, 1130 (2012).
- [7] B. Nachman, D. Provasoli, W. A. de Jong, and C. W.

- Bauer, Phys. Rev. Lett. **126**, 062001 (2021).
- [8] A. A. Abrikosov, L. P. Gorkov, and I. E. Dzyaloshinski, *Methods of quantum field theory in statistical physics* (Courier Corporation, 2012).
- [9] A. Szabo and N. S. Ostlund, *Modern Quantum Chemistry: Introduction to Advanced Electronic Structure Theory* (Courier Corporation, 2012).
- [10] R. Orús, Nature Reviews Physics **1**, 538 (2019).
- [11] J. Jordan, R. Orús, G. Vidal, F. Verstraete, and J. I. Cirac, Physical review letters **101**, 250602 (2008).
- [12] D. Sholl and J. A. Steckel, *Density Functional Theory: a Practical Introduction* (John Wiley & Sons, 2011).
- [13] G. Knizia and G. K.-L. Chan, Physical review letters **109**, 186404 (2012).
- [14] N. C. Rubin, arXiv preprint arXiv:1610.06910 (2016).
- [15] W. Li, Z. Huang, C. Cao, Y. Huang, Z. Shuai, X. Sun, J. Sun, X. Yuan, and D. Lv, arXiv preprint arXiv:2109.08062 (2021).
- [16] B. Bauer, D. Wecker, A. J. Millis, M. B. Hastings, and M. Troyer, Phys. Rev. X **6**, 031045 (2016).
- [17] D. M. Ceperley and B. J. Alder, Physical review letters **45**, 566 (1980).
- [18] S. Zhang, J. Carlson, and J. E. Gubernatis, Physical Review B **55**, 7464 (1997).
- [19] G. H. Booth, A. J. Thom, and A. Alavi, The Journal of chemical physics **131**, 054106 (2009).
- [20] G. Carleo and M. Troyer, Science **355**, 602 (2017).
- [21] J. Hermann, Z. Schätzle, and F. Noé, Nature Chemistry **12**, 891 (2020).
- [22] D. Pfau, J. S. Spencer, A. G. Matthews, and W. M. C. Foulkes, Physical Review Research **2**, 033429 (2020).
- [23] Y. S. Al-Hamdani, P. R. Nagy, A. Zen, D. Barton, M. Kállay, J. G. Brandenburg, and A. Tkatchenko, Nature Communications **12**, 1 (2021).
- [24] M. Troyer and U.-J. Wiese, Physical review letters **94**, 170201 (2005).
- [25] M. A. Nielsen and I. Chuang, *Quantum computation and quantum information* (American Association of Physics Teachers, 2002).
- [26] T. Albash and D. A. Lidar, Reviews of Modern Physics **90**, 015002 (2018).
- [27] A. Y. Kitaev, arXiv preprint quant-ph/9511026 (1995).
- [28] D. S. Abrams and S. Lloyd, Physical Review Letters **83**, 5162 (1999).
- [29] A. Aspuru-Guzik, A. D. Dutoi, P. J. Love, and M. Head-Gordon, Science **309**, 1704 (2005).
- [30] L. Lin and Y. Tong, PRX Quantum **3**, 010318 (2022).
- [31] K. Wan, M. Berta, and E. T. Campbell, Physical Review Letters **129**, 030503 (2022).
- [32] P. Zeng, J. Sun, and X. Yuan, (2021), arXiv:2109.15304 [quant-ph].
- [33] M. Huo and Y. Li, (2021), arXiv:2109.07807 [quant-ph].
- [34] Y. Dong, L. Lin, and Y. Tong, PRX Quantum **3**, 040305 (2022).
- [35] Y. Ge, J. Tura, and J. I. Cirac, Journal of Mathematical Physics **60**, 022202 (2019), <https://doi.org/10.1063/1.5027484>.
- [36] S. Lu, M. C. Bañuls, and J. I. Cirac, PRX Quantum **2**, 020321 (2021).
- [37] J. Preskill, Quantum **2**, 79 (2018).
- [38] E. Altman, K. R. Brown, G. Carleo, L. D. Carr, E. Demler, C. Chin, B. DeMarco, S. E. Economou, M. A. Eriksson, K.-M. C. Fu, M. Greiner, K. R. Hazzard, R. G. Hulet, A. J. Kollár, B. L. Lev, M. D. Lukin, R. Ma, X. Mi, S. Misra, C. Monroe, K. Murch, Z. Nazario, K.-K. Ni, A. C. Potter, P. Roushan, M. Saffman, M. Schleier-Smith, I. Siddiqi, R. Simmonds, M. Singh, I. Spielman, K. Temme, D. S. Weiss, J. Vučković, V. Vuletić, J. Ye, and M. Zwierlein, PRX Quantum **2**, 017003 (2021).
- [39] S. Endo, Z. Cai, S. C. Benjamin, and X. Yuan, Journal of the Physical Society of Japan **90**, 032001 (2021), <https://doi.org/10.7566/JPSJ.90.032001>.
- [40] M. Cerezo, A. Poremba, L. Cincio, and P. J. Coles, Quantum **4**, 248 (2020).
- [41] K. Bharti, A. Cervera-Lierta, T. H. Kyaw, T. Haug, S. Alperin-Lea, A. Anand, M. Degroote, H. Heimonen, J. S. Kottmann, T. Menke, W.-K. Mok, S. Sim, L.-C. Kwek, and A. Aspuru-Guzik, Rev. Mod. Phys. **94**, 015004 (2022).
- [42] D. Cleland, G. H. Booth, and A. Alavi, The Journal of chemical physics **132**, 041103 (2010).
- [43] (See Supplementary Materials for a more detailed introduction to the background of VQA and QMC, the sign problem, QC-FCIQMC, and more simulation results.).
- [44] A. Peruzzo, J. McClean, P. Shadbolt, M.-H. Yung, X.-Q. Zhou, P. J. Love, A. Aspuru-Guzik, and J. L. O'Brien, Nature communications **5**, 1 (2014).
- [45] H. R. Grimsley, S. E. Economou, E. Barnes, and N. J. Mayhall, Nature comm. **10**, 1 (2019).
- [46] A. Abbas, D. Sutter, C. Zoufal, A. Lucchi, A. Figalli, and S. Woerner, Nature Computational Science **1**, 403 (2021).
- [47] Z. Holmes, K. Sharma, M. Cerezo, and P. J. Coles, (2021), arXiv:2101.02138 [quant-ph].
- [48] E. R. Anschuetz and B. T. Kiani, arXiv preprint arXiv:2205.05786 (2022).
- [49] M. Cerezo and P. J. Coles, arXiv e-prints, arXiv (2020).
- [50] S. Wang, E. Fontana, M. Cerezo, K. Sharma, A. Sone, L. Cincio, and P. J. Coles, Nature Communications **12** (2021), 10.1038/s41467-021-27045-6.
- [51] L. Bittel and M. Kliesch, Phys. Rev. Lett. **127**, 120502 (2021).
- [52] J. Klassen, M. Marvian, S. Piddock, M. Ioannou, I. Hen, and B. M. Terhal, SIAM Journal on Computing **49**, 1332 (2020), <https://doi.org/10.1137/19M1287511>.
- [53] D. Hangleiter, I. Roth, D. Nagaj, and J. Eisert, Science advances **6**, eabb8341 (2020).
- [54] G. Torlai, J. Carrasquilla, M. T. Fishman, R. G. Melko, and M. P. A. Fisher, Phys. Rev. Research **2**, 032060 (2020).
- [55] R. Levy and B. K. Clark, Phys. Rev. Lett. **126**, 216401 (2021).
- [56] (Note that the upper bounds of Theorem 1 and 2 are not tight, and the NSI could be much smaller in reality.).
- [57] K. M. Nakanishi, K. Mitarai, and K. Fujii, Phys. Rev. Research **1**, 033062 (2019).
- [58] R. M. Parrish, E. G. Hohenstein, P. L. McMahan, and T. J. Martínez, Phys. Rev. Lett. **122**, 230401 (2019).
- [59] (One may argue that why we need QMC if we could already diagonalize  $H$ . The motivation is that exactly diagonalizing  $H$  might need a deep quantum circuit, which is beyond the capability of near-term quantum devices. Contrarily, we only need to approximately diagonalize  $H$  with a shallower circuit and apply QMC to further improve the accuracy.).
- [60] Z.-J. Zhang, T. H. Kyaw, J. Kottmann, M. Degroote, and A. Aspuru-Guzik, Quantum Science and Technol-

- ogy (2021).
- [61] H. L. Tang, V. Shkolnikov, G. S. Barron, H. R. Grimsley, N. J. Mayhall, E. Barnes, and S. E. Economou, arXiv preprint arXiv:1911.10205 (2019).
- [62] H. L. Tang, V. Shkolnikov, G. S. Barron, H. R. Grimsley, N. J. Mayhall, E. Barnes, and S. E. Economou, PRX Quantum **2**, 020310 (2021).
- [63] Y. Fan, C. Cao, X. Xu, Z. Li, D. Lv, and M.-H. Yung, arXiv preprint arXiv:2106.15210 (2021).
- [64] (Note that we can reuse the result of  $|H_{ji}|$  and  $H_{ji}/|H_{ji}|$ , if we have already obtained them in previous steps.)
- [65] (All the energy and standard deviation are evaluated by taking energies after reaching a certain total evolution time, and usually after the total number of walkers stabilizes.)
- [66] D. Wecker, M. B. Hastings, and M. Troyer, Physical Review A **92**, 042303 (2015).
- [67] C. Cade, L. Mineh, A. Montanaro, and S. Stanisic, Physical Review B **102**, 235122 (2020).
- [68] Z. Cai, Physical Review Applied **14**, 014059 (2020).
- [69] N. Blunt, S. D. Smart, J. Kersten, J. Spencer, G. H. Booth, and A. Alavi, The Journal of chemical physics **142**, 184107 (2015).
- [70] A. A. Holmes, N. M. Tubman, and C. Umrigar, Journal of chemical theory and computation **12**, 3674 (2016).
- [71] J. B. Schriber and F. A. Evangelista, The Journal of chemical physics **144**, 161106 (2016).
- [72] N. M. Tubman, J. Lee, T. Y. Takeshita, M. Head-Gordon, and K. B. Whaley, The Journal of chemical physics **145**, 044112 (2016).
- [73] Z.-X. Li and H. Yao, Annual Review of Condensed Matter Physics **10**, 337 (2019).
- [74] W. J. Huggins, B. A. O’Gorman, N. C. Rubin, D. R. Reichman, R. Babbush, and J. Lee, Nature **603**, 416 (2022).
- [75] X. Xu and Y. Li, arXiv e-prints , arXiv:2205.14903 (2022), arXiv:2205.14903 [quant-ph].
- [76] G. Mazzola and G. Carleo, arXiv e-prints , arXiv:2205.09203 (2022), arXiv:2205.09203 [quant-ph].
- [77] T. L. Patti, O. Shehab, K. Najafi, and S. F. Yelin, arXiv e-prints , arXiv:2112.02190 (2021), arXiv:2112.02190 [quant-ph].
- [78] S. Wouters, B. Verstichel, D. Van Neck, and G. K.-L. Chan, Physical Review B **90**, 045104 (2014).
- [79] A. W. Sandvik and H. G. Evertz, Physical Review B **82**, 024407 (2010).
- [80] B. K. Clark and H. J. Changlani, arXiv preprint arXiv:1404.2296 (2014).
- [81] S. B. Bravyi and A. Y. Kitaev, Annals of Physics **298**, 210 (2002).
- [82] J. T. Seeley, M. J. Richard, and P. J. Love, The Journal of chemical physics **137**, 224109 (2012).
- [83] J. Romero, R. Babbush, J. R. McClean, C. Hempel, P. J. Love, and A. Aspuru-Guzik, Quantum Science and Technology **4**, 014008 (2018).
- [84] I. D. Kivlichan, J. McClean, N. Wiebe, C. Gidney, A. Aspuru-Guzik, G. K.-L. Chan, and R. Babbush, Physical review letters **120**, 110501 (2018).
- [85] S. Bravyi, D. P. Divincenzo, R. I. Oliveira, and B. M. Terhal, arXiv preprint quant-ph/0606140 (2006).
- [86] M. Iazzi, A. A. Soluyanov, and M. Troyer, Physical Review B **93**, 115102 (2016).
- [87] R. Levy and B. K. Clark, Physical review letters **126**, 216401 (2021).
- [88] L. Gupta and I. Hen, Advanced Quantum Technologies **3**, 1900108 (2020).
- [89] M. Marvian, D. A. Lidar, and I. Hen, Nature communications **10**, 1 (2019).
- [90] J. R. McClean, S. Boixo, V. N. Smelyanskiy, R. Babbush, and H. Neven, Nature communications **9**, 1 (2018).
- [91] W. Hoeffding, Journal of the American statistical association **58**, 13 (1963).
- [92] I. G. Ryabinkin, R. A. Lang, S. N. Genin, and A. F. Izmaylov, Journal of chemical theory and computation **16**, 1055 (2020).
- [93] N. C. Rubin, J. Lee, and R. Babbush, Journal of Chemical Theory and Computation **18**, 1480 (2022).
- [94] L. Lin and Y. Tong, Quantum **4**, 372 (2020).
- [95] G. Wang, D. Stilck-França, R. Zhang, S. Zhu, and P. D. Johnson, arXiv preprint arXiv:2209.06811 (2022).
- [96] G. A. Quantum, Collaborators\*†, F. Arute, K. Arya, R. Babbush, D. Bacon, J. C. Bardin, R. Barends, S. Boixo, M. Broughton, B. B. Buckley, *et al.*, Science **369**, 1084 (2020).
- [97] S. Stanisic, J. L. Bosse, F. M. Gambetta, R. A. Santos, W. Mruczkiewicz, T. E. O’Brien, E. Ostby, and A. Montanaro, Nature Communications **13**, 5743 (2022).
- [98] T. E. O’Brien, G. Anselmetti, F. Gkritis, V. Elfving, S. Polla, W. J. Huggins, O. Oumarou, K. Kechedzhi, D. Abanin, R. Acharya, *et al.*, arXiv preprint arXiv:2210.10799 (2022).
- [99] S. Guo, J. Sun, H. Qian, M. Gong, Y. Zhang, F. Chen, Y. Ye, Y. Wu, S. Cao, K. Liu, *et al.*, arXiv preprint arXiv:2212.08006 (2022).
- [100] E. Campbell, Physical review letters **123**, 070503 (2019).

## BACKGROUND

In this section, we give a more detailed background introduction to variational quantum algorithms and quantum Monte Carlo.

### Variational Quantum Eigensolver

We focus on variational quantum eigensolver (VQE) as a typical example of general variational quantum algorithms [37–41]. VQE is a hybrid quantum-classical method that utilizes quantum devices to prepare parameterized quantum circuits and optimize the parameters classically [44]. Through encoding the cost function, usually the corresponding Hamiltonian for the system of interest, one is able to estimate its expectation value by measuring the quantum state. In the following discussion, we focus on fermionic Hamiltonians. Yet, our results apply for general Hamiltonians. For a fermionic Hamiltonian, we use the Jordan-Wigner encoding which encodes the occupation numbers of the spin orbitals to qubits. The alternatives to JW encoding include the parity transformation and Bravyi-Kitaev transformation [81, 82].

Several carefully designed ansatz is proposed for the specific quantum systems concerning their unique properties. In this work, we focus on two types of algorithms: the ADAPT-VQE [45], and the Hamiltonian Variational Ansatz (HVA) [66–68].

ADAPT-VQE algorithms have been put forward as general protocols for adaptively growing the ansatz. The ADAPT-VQE methods build the quantum circuit iteratively by adding the operator from the operator pool with the largest gradient with respect to the loss function of the current circuit at every iteration. After adding a new operator to the circuit, one variationally optimizes the new parameter while also re-optimize all previous parameters. An iteration terminates when the norm of the gradient is smaller than a certain threshold. Several variations for this algorithm have been proposed with distinct features. The most commonly adopted operator pool is constructed according to the unitary coupled cluster ansatz with single and double excitations (UCCSD) [83]. For a molecular non-relativistic Hamiltonian of the form

$$H = H_0 + \sum_{pq} h_{pq} a_p^\dagger a_q + \frac{1}{2} \sum_{pqrs} h_{pqrs} a_p^\dagger a_q^\dagger a_r a_s, \quad (7)$$

where  $h_{pq}$  and  $h_{pqrs}$  are coefficients obtained from one- and two-electron integrals, the coupled cluster method with single and double excitation heuristic truncated the higher excitations and gives the following ansatz based upon Hartree-Fock orbitals:

$$|\psi_{CCSD}\rangle = e^{T_1+T_2} |\psi_{HF}\rangle. \quad (8)$$

Here  $T_1$  and  $T_2$  correspond to single and double excitations:

$$T_1 = \sum_{i \in occ, k \in virt} t_i^k a_i^\dagger a_k \quad (9)$$

and

$$T_2 = \sum_{i > j \in occ, k > l \in virt} t_{ij}^{kl} a_i^\dagger a_j^\dagger a_k a_l \quad (10)$$

The operator  $e^T$  cannot be implemented on a quantum computer due to its non-unitarity. However, its variant  $e^{T-T^\dagger}$  is unitary for a given excitation operator  $T$ . This is dubbed the unitary coupled cluster ansatz. Therefore, the operator pool for the ADAPT-VQE ansatz is formed by the single and double excitation operators from  $T_1$  and  $T_2$  but every term has to subtract its conjugate transpose. Later we will use this ansatz to construct the VQE basis for the nitrogen molecule.

The HVA ansatz is particularly suitable for the Hubbard model. The Hubbard models are celebrated for modeling strong-correlated electronic effects in many-body quantum physics. The model captures the competition between electronic hopping and on-site repulsion, which as the form

$$H = - \sum_{i,j} t_{ij} \sum_{\sigma=\uparrow,\downarrow} a_{i\sigma}^\dagger a_{j\sigma} + U \sum_i n_{i\uparrow} n_{i\downarrow}, \quad (11)$$



where  $t$  and  $U$  is the hopping and repulsion strength, and  $n_i$  denotes the number operator. For a square lattice, the HVA algorithm separates the Hamiltonian into three parts  $H = H_v + H_h + H_U$ . The former two terms are the hopping terms in Eq. (11) in the vertical and horizontal direction, and the last one is the on-site term. For a reference state  $|\psi_{\text{ref}}\rangle$ , the ansatz takes the following form

$$\Psi = \prod_{b=1}^B \left[ \exp\left(i\frac{\theta_U^b}{2}H_U\right) \exp\left(i\frac{\theta_h^b}{2}H_h\right) \exp\left(i\frac{\theta_v^b}{2}H_v\right) \exp\left(i\frac{\theta_U^b}{2}H_U\right) \right] |\psi_{\text{ref}}\rangle, \quad (12)$$

where  $\theta$  are parameters for the ansatz, and  $B$  is the total iteration. With recent progress [84], one notices that the one-body terms in the ansatz can be compiled exactly without trotterization for they have the fermionic Gaussian form.

### Quantum Monte Carlo

Quantum Monte Carlo (QMC) is a class of classical computation algorithms that invokes the Monte Carlo method to approximate properties of quantum many-body systems. Projector quantum Monte Carlo is a subclass of QMC attempting to stochastically apply walkers to follow the imaginary-time evolution, which however generally causes the infamous sign problem in fermionic systems. The sign problem can be alleviated through different approximations, such as the fix-node approximation in Diffusion Monte Carlo (DMC) and the phaseless approximation in auxiliary-field quantum Monte Carlo (AFQMC). However, most techniques introduce bias while trying to ease the sign problem. In this work, we seek to alleviate the sign problem without introducing bias to the solution by combining quantum computing with a QMC algorithm.

A hybrid algorithm of AFQMC and quantum computing has been proposed in Ref. [74] where they prepared a non-trivial trial state for AFQMC with the quantum device. Shadow tomography is implemented on the quantum device to calculate the overlaps between the trial state and stochastic walker states, which are the values required for energy estimation. These overlaps are easy to estimate to an additive error and friendly for virtual correlation energy calculation without overhead on quantum devices. However, estimation of ground state energy to an additive error with the scheme in its current form requires overlap estimation to a relative error, which can be hard when some of the overlaps vanish exponentially fast as the size of the system increases. Here in this work, we circumvent the overlap estimation by combining quantum computing with another type of projector QMC algorithm in the space of Slater determinants, called the full-configuration interaction quantum Monte Carlo (FCIQMC) algorithm [19, 42]. The FCIQMC algorithm pursues FCI-level accuracy estimation of ground-state properties with fewer resources. Now we describe its main procedure as follows.

Suppose that the wavefunction is decomposed as follows,

$$|\psi(\tau)\rangle = \sum_i c_i(\tau) |i\rangle \quad (13)$$

where  $\tau$  is the imaginary time we are evolving and  $|i\rangle$ s are the Fock basis states, which corresponds to the single determinant configurations in the fermionic representation. Substituting this into the imaginary time Schrodinger equation

$$|\psi(\tau)\rangle \propto e^{-H\tau} |\psi(0)\rangle, \quad (14)$$

taking the first-order approximation, one obtains a set of coupled differential equations for the evolution of coefficients  $c_i$ s:

$$-\frac{dc_i(\tau)}{d\tau} = \sum_j (H_{ij} - S\delta_{ij})c_j(\tau) \quad (15)$$

where  $H_{ij}$ s are the Hamiltonian matrix elements under a certain basis (here the Fock basis) and  $S$  is an additional energy shift on the diagonal terms. One usually starts with the Hartree-Fock energy and adjusts the value along the evolution for the purpose of walker population control. Empirical formulas are proposed in Ref. [19] for the adjustment of  $S$  as follows

$$S(\tau) = S(\tau - A\Delta\tau) - \frac{\zeta}{A\Delta\tau} \ln \frac{N(\tau)}{N(\tau - A\Delta\tau)}, \quad (16)$$

where  $N$  is the total walker number at a specific time,  $A$  and  $\zeta$  are values one can adjust according to the system of interest.

FCIQMC considers a set of walkers, who live in computational basis vector space with coefficients being  $\pm 1$ . The population  $N_i(\tau)$  at each basis vector  $|i\rangle$  is therefore an integer, obtained by the signed sum of all walkers located at this basis vector. One needs to design the QMC algorithm such that  $N_i(\tau)$  is proportional to the corresponding amplitude  $c_i(\tau)$  following the imaginary time dynamics. Hence, if one trotterize the time evolution into steps of size  $\Delta\tau$ , the FCIQMC algorithm consists of the following three steps at each time step according to eq. (53):

- Spawning: For each walker living in  $|i\rangle$ , spawn a child walker  $|j\rangle$  ( $j \neq i$ ) with probability  $|H_{ij}|\Delta\tau$  up to a normalization constant. Moreover, if this quantity  $H_{ij}$  is positive, then the child has the same sign as the parent, and the opposite sign otherwise.
- Death/clone: If the quantity  $H_{ii} - S > 0$ , then walker  $|\phi_i\rangle$  dies with probability  $(H_{ii} - S)\Delta\tau$ ; and if  $H_{ii} - S < 0$ , then the walker clones itself with probability  $|(H_{ii} - S)|\Delta\tau$ .
- Annihilation: As we have alluded to, we want the signed sum of walkers to be proportional to the true amplitudes. Therefore, at the end of each time step, we take the signed sum of walkers at each basis vector and annihilate every pair of walkers with opposite signs.

### SIGN PROBLEM IN QUANTUM MONTE CARLO

In this section, we give a more detailed analysis of the sign problem in QMC. We consider the non-stoquasticity indicator and derive its upper bounds for different cases.

#### Definition and Mitigation of The Sign Problem

The projector QMC methods are plagued by the sign problem. We briefly discuss the implications of the sign problem in the main text, and here we give a self-contained introduction and proofs of the bounds of the sign problem. As we intend to implement the imaginary time evolution (ITE) operator to an initial state, we have to normalize the resultant state due to the non-unitarity of the ITE operator. In cases of the projector QMC methods, we represent the overall wave function as a distribution of walker states over the chosen basis, and the walkers evolve upon implementing the ITE operator. The sign problem manifests when computing the expectation value of observable with the final-round walkers as we normalize the wave function in the chosen basis. To see this, let us compute the partition function of the ITE operator on the chosen basis. Here, we first consider the Fock basis for fermionic systems, and we get

$$\begin{aligned} \text{Tr}(e^{-\beta H}) &= \sum_{k=0}^{\infty} \frac{(-\beta)^k}{k!} \text{Tr}(H^k) \\ &= \sum_{k=0}^{\infty} \frac{(-\beta)^k}{k!} \sum_{\{|\zeta\rangle\}} \langle \zeta_0 | H | \zeta_1 \rangle \langle \zeta_1 | H | \zeta_2 \rangle \cdots \langle \zeta_{k-1} | H | \zeta_0 \rangle. \end{aligned} \quad (17)$$

Here,  $\{|\zeta\rangle\}$  is a set of complete orthogonal basis, i.e., the Fock basis in our case. Eq. (17) gives us the path integral form of the partition function, which consists of all cyclic paths in the chosen basis. One notices that both positive and negative paths could contain in Eq. (17). By definition of the sign problem, the system is sign-problem-free if all the paths are positive in Eq. (17) [24]. In particular, fermionic systems are known to be notoriously affected by the sign problem because the cyclic paths include cases where odd pairs of particles are exchanged, which changes the sign of the paths. The standard way to deal with the negative path is to sample according to its absolute value in Monte Carlo simulation. To quantify the sign problem, we follow the deduction of Troyer and Wiese [24] and consider computing the expectation value of the operator  $A$  with respect to the thermal state in a similar form

$$\begin{aligned} \langle A \rangle &= \frac{\text{Tr}[Ae^{-\beta H}]}{\text{Tr}[e^{-\beta H}]} = \frac{\text{Tr}[Ae^{\beta G}]}{\text{Tr}[e^{\beta G}]} = \frac{\sum_{k=0}^{\infty} \frac{\beta^k}{k!} \sum_{i_0, i_1, \dots, i_k} A_{i_0 i_1} G_{i_1 i_2} \cdots G_{i_k i_0}}{\sum_{k=0}^{\infty} \frac{\beta^k}{k!} \sum_{i_1, i_2, \dots, i_k} G_{i_1 i_2} G_{i_2 i_3} \cdots G_{i_k i_1}} \\ &= \frac{\sum_{k=0}^{\infty} \frac{\beta^k}{k!} \sum_{i_0, i_1, \dots, i_k} A_{i_0 i_1} |G_{i_1 i_2} \cdots G_{i_k i_0}| s_{i_1 \cdots i_k, i_0} / \sum_{i_1, i_2, \dots, i_k} |G_{i_1 i_2} \cdots G_{i_k i_0}|}{\sum_{k=0}^{\infty} \frac{\beta^k}{k!} \sum_{i_1, i_2, \dots, i_k} |G_{i_1 i_2} G_{i_2 i_3} \cdots G_{i_k i_1}| s_{i_1 \cdots i_k, i_1} / \sum_{i_1, i_2, \dots, i_k} |G_{i_1 i_2} \cdots G_{i_k i_1}|} = \frac{\langle As \rangle}{\langle s \rangle}, \end{aligned} \quad (18)$$

where  $G$  is the same as in the main text, which equals to  $\alpha I - H$  with  $\alpha = \max_i H_{ii}$ , and we extract the sign of  $G_{i_1 i_2} G_{i_2 i_3} \cdots G_{i_k i_1}$  as  $s_{i_1 \dots i_k, i_1}$ . In cases where all off-diagonal terms in the Hamiltonian are non-positive, the system is sign-problem-free as can be seen from Eq. (18), and these kinds of Hamiltonians are dubbed as “stoquastic” [85] or “Bosonic”. We notice that the denominator is the average sign  $\langle s \rangle$  in Eq. (18) is the ratio of the partition function and its bosonic counterpart. By definition of the partition function that is exponential of the free energy, the average sign goes down exponentially as  $\exp(-\beta n \Delta f)$ , where  $\Delta f$  is the free energy difference between the original and its bosonic form system. Upon computing the expectation of an observable, the estimator is enlarged exponentially by the partition function, so as its variance

$$\frac{\Delta s}{\langle s \rangle} = \frac{\sqrt{(\langle s^2 \rangle - \langle s \rangle^2)/M}}{\langle s \rangle} = \frac{\sqrt{1 - \langle s \rangle^2}}{\sqrt{M} \langle s \rangle} \propto \frac{e^{\beta n \Delta f}}{\sqrt{M}}. \quad (19)$$

This means that the requiring number  $M$  of sampled walkers needs to grow exponentially to counterbalance the variance growth. In practice, because we can only afford a finite size of samples, the sign problem often manifests itself as great statistical fluctuation in the observable estimation step. Note that it is generally hard to resolve the sign problem as Troyer and Wieser [24] proved that the problem is **NP**-complete. In certain cases, the sign problem can be shown to be removed by a local transformation or basis rotation. However, the intrinsic hardness of solving the sign problem is characterized by their topological nature [86], and hence local transformations are not capable of curing the sign problem in the most general cases.

It is natural to think of easier ways to quantify the sign problem other than the path integral form in Eq. (17), and ways to mitigate the sign problem. It is also of independent interest to develop measures for the sign problem as they serve as loss functions for mitigating the sign problem [53, 87], which is of great significance for extending numerical ability in classical QMC simulation of quantum many-body systems and materials. The criteria for the measure of the sign problem include i) faithfully reflect the severity of the sign problem for a Hamiltonian in a given basis, e.g. deviation of the sample complexity for the Hamiltonian from that of the effective bosonic form Hamiltonian; ii) general enough that it is independent of the details of implantation of the QMC algorithms; iii) efficiently computable. The non-stoquasticity, being directly related to the Hamiltonian and a computationally tractable description of the sign problem, is adopted as the measure in Ref. [53]. The authors also provide numerical evidence with randomly generated Hamiltonians for supporting the statement that the non-stoquasticity measures the severity of the sign problem. However, as pointed out in Ref. [88] that the off-diagonal terms do not directly induce the sign problem, but the cumulative phases of the cyclic paths in the path-integral expression do. Unfortunately, it is left unanswered to what extent the non-stoquasticity (quantitatively) contributes to the sign problem. Furthermore, it is desirable to propose a measure other than the cumulative phases as there are exponentially many of them. In the next section, we derive rigorously the measure of the sign problem following the criteria discussed above. It is found that the upper bound for the overall effect of path-integral for the negative cyclic paths (i.e., the direct origin of the sign problem) adds up to be directly related to the negative and positive off-diagonal terms in the Hamiltonian separately. This renders our measure very much like the properties of non-stoquasticity, and we thus name the measure as non-stoquasticity indicator (NSI). Our result elucidates the relationship between non-stoquasticity and the measure of severity of the sign problem. We discuss this in detail in the next section.

To suppress the sign problem without altering the spectrum of the Hamiltonian, the general way is to implement similarity transformation with a unitary operator  $U(\vec{\theta})$  [53]

$$H_T(\vec{\theta}) = U(\vec{\theta})^\dagger H U(\vec{\theta}). \quad (20)$$

Generally speaking, an arbitrary unitary will scramble the original Hamiltonian, i.e., the Hamiltonian will become highly non-local. As a consequence, it is not possible to implement the ITE operator both in classical and quantum cases. To preserve the locality after the transformation, several proposals [53, 87, 89] have been put forward. For spin systems, local Clifford and special orthogonal group [53, 89] transformation have been considered. The former is due to the fact that the Pauli group is the normal subgroup of the Clifford group, and the latter will only scramble the observable locally while maintaining its elements real. For fermionic systems, the basis rotation transformations [87] are ideal choices as they shall not alter the locality. However, both the three types of transformations are limited in their expressive power, and basically, it is **NP**-complete [53, 89] to find the curing transformation in these settings. The above-mentioned three types of transformations are efficient-simulatable classically. To further extend the capacity of mitigating the sign problem, we suggest thinking of similarity transformation realized by quantum computing-related protocols as quantum circuits are natural building blocks to construct arbitrary unitaries. As we will discuss in the next session, we propose to alter the basis from the Fock basis to the VQE-rotated basis, which is  $\{|\phi_i\rangle \equiv U(\vec{\theta})|\zeta_i\rangle\}$  with  $U(\vec{\theta})$  prepared by the VQE algorithm. Let us consider the path integral form of the partition function in the

VQE-rotated basis

$$\begin{aligned} & \sum_{k=0}^{\infty} \frac{(-\beta)^k}{k!} \sum_{\{|\zeta\rangle\}} \langle \zeta_0 | U(\vec{\theta})^\dagger H U(\vec{\theta}) | \zeta_1 \rangle \langle \zeta_1 | U(\vec{\theta})^\dagger H U(\vec{\theta}) | \zeta_2 \rangle \cdots \langle \zeta_{k-1} | U(\vec{\theta})^\dagger H U(\vec{\theta}) | \zeta_0 \rangle \\ & = \sum_{k=0}^{\infty} \frac{(-\beta)^k}{k!} \text{Tr}(H_T(\vec{\theta})^k) = \text{Tr}(e^{-\beta H_T(\vec{\theta})}), \end{aligned} \quad (21)$$

which matches the general way to suppress the sign problem as Eq. (20). From this perspective, our algorithms allow an effective implementation of a rather complicated unitary to realize Eq. (20) without actually scrambling the Hamiltonian. Therefore, with the similarity transformation effectively implemented by a quantum circuit, we expect our approach to achieving better performance in easing the sign problem, and we provide quantitative measures for gauging the sign problem in the following.

### Non-Stoquasticity Indicator For Real Hamiltonians

For any given Hamiltonian  $H$ , we refer to  $\tilde{H}$  Bosonic form of the original Hamiltonian, which has the following form

$$\begin{aligned} \tilde{H}_{ij} &= -|H_{ij}|, & \text{if } i \neq j; \\ \tilde{H}_{ij} &= H_{ij}, & \text{otherwise.} \end{aligned} \quad (22)$$

To see the relationship between the severity of the sign problem and the non-stoquasticity of the Hamiltonian after the similarity transformation, we derive an easily computing formula by relating it to the partition function difference between  $H_T$  and its Bosonic form  $\tilde{H}_T$ . We refer this quantity to the Non-Stoquasticity Indicator (NSI),  $S(H)$  for any given Hamiltonian  $H$  spanned by the basis  $\{|\phi\rangle\}$ , which has the form

$$\begin{aligned} S(H) &= \text{Tr}(e^{-\beta \tilde{H}}) - \text{Tr}(e^{-\beta H}) \\ &= \text{Tr}(e^{-\beta(\alpha I - \tilde{G})}) - \text{Tr}(e^{-\beta(\alpha I - G)}) \\ &= e^{-\beta\alpha} \left( \sum_{k=0}^{\infty} \frac{\beta^k}{k!} \sum_{\{|\phi\rangle\}} (|\langle \phi_0 | G | \phi_1 \rangle \langle \phi_1 | G | \phi_2 \rangle \cdots \langle \phi_{k-1} | G | \phi_0 \rangle| - \langle \phi_0 | G | \phi_1 \rangle \langle \phi_1 | G | \phi_2 \rangle \cdots \langle \phi_{k-1} | G | \phi_0 \rangle) \right) \end{aligned} \quad (23)$$

Note that the diagonal terms in  $G$  are all non-negative. We claim that the NSI is essentially the most general form that accounts for all possible negative paths in the path-integral formula for measuring the severity of the sign problem.

To arrive at the final expression for the NSI, we need to sort out all the negative path integrals in Eq. (23). We define  $H_+$  and  $H_-$  as

$$\begin{aligned} (H_+)_{ij} &= H_{ij}, \text{ if } H_{ij} > 0 \text{ and } i \neq j; (H_+)_{ij} = 0, \text{ otherwise;} \\ (H_-)_{ij} &= H_{ij}, \text{ if } H_{ij} < 0 \text{ or } i = j; (H_-)_{ij} = 0, \text{ otherwise.} \end{aligned} \quad (24)$$

According to the above definition, the corresponding  $G$  will be

$$\begin{aligned} G_+ &= \alpha - H_-; \\ G_- &= \alpha - H_+. \end{aligned} \quad (25)$$

We first focus on cases where all terms in the given Hamiltonian  $H$  are real. The NSI is supposed to be  $-2$ -fold of sum of all negative path integrals

$$\begin{aligned} & S(H)/e^{-\beta\alpha} \\ &= -2 \sum_{k=0}^{\infty} \frac{(\beta)^{2k+1}}{(2k+1)!} \sum_{\{\eta_1, \eta_2\}} \left( G_-^{(1)}(\eta_1|\eta_2) G_+^{(2k)}(\eta_2|\eta_1) + G_-^{(3)}(\eta_1|\eta_2) G_+^{(2k-2)}(\eta_2|\eta_1) + \cdots + G_-^{(2k+1)}(\eta_1|\eta_1) \right) \\ & \quad - 2 \sum_{k=0}^{\infty} \frac{(\beta)^{2k}}{(2k)!} \sum_{\{\eta_1, \eta_2\}} \left( G_-^{(1)}(\eta_1|\eta_2) G_+^{(2k-1)}(\eta_2|\eta_1) + G_-^{(3)}(\eta_1|\eta_2) G_+^{(2k-3)}(\eta_2|\eta_1) + \cdots + G_-^{(2k-1)}(\eta_1|\eta_2) G_+^{(1)}(\eta_2|\eta_1) \right), \end{aligned} \quad (26)$$

where  $G_{-/+}^{(i)}$  stands for the path integral that contains  $i$  positive/negative elements from matrix  $G$ , and we sum over all the possible set of paths denote by  $\eta_1, \eta_2$  that contains the right amount of positive and negative components. The path integral form is equivalent to choosing elements from  $G_-$  and  $G_+$ , and we have

$$\begin{aligned} &= 2 \sum_{k=0}^{\infty} \frac{(\beta)^{2k+1}}{(2k+1)!} \left( \binom{2k+1}{1} \|G_-\|_{L_1} \|G_+^{2k}\|_{L_1} + \binom{2k+1}{3} \|G_-^3\|_{L_1} \|G_+^{2k-2}\|_{L_1} + \cdots + \binom{2k+1}{2k+1} \|G_-^{2k+1}\|_{L_1} \right) \\ &+ 2 \sum_{k=0}^{\infty} \frac{(\beta)^{2k}}{(2k)!} \left( \binom{2k}{1} \|G_-\|_{L_1} \|G_+^{2k-1}\|_{L_1} + \binom{2k}{3} \|G_-^3\|_{L_1} \|G_+^{2k-3}\|_{L_1} + \cdots + \binom{2k}{2k-1} \|G_-^{2k-1}\|_{L_1} \|G_+\|_{L_1} \right). \end{aligned} \quad (27)$$

For  $L_1$  norm of some matrix  $x$ , its  $L_1$  norm of  $m$ th power is no larger than its  $L_1$  norm's  $m$ th power for any positive integer  $m$ , which is  $\|x^m\|_{L_1} \leq \|x\|_{L_1}^m$ . We get the upper bound for the NSI,

$$\begin{aligned} &\leq 2 \sum_{k=0}^{\infty} \frac{(\beta)^{2k+1}}{(2k+1)!} \left( \binom{2k+1}{1} \|G_-\|_{L_1} \|G_+\|_{L_1}^{2k} + \binom{2k+1}{3} \|G_-\|_{L_1}^3 \|G_+\|_{L_1}^{2k-2} + \cdots + \binom{2k+1}{2k+1} \|G_+\|_{L_1}^{2k+1} \right) \\ &+ 2 \sum_{k=0}^{\infty} \frac{(\beta)^{2k}}{(2k)!} \left( \binom{2k}{1} \|G_-\|_{L_1} \|G_+\|_{L_1}^{2k-1} + \binom{2k}{3} \|G_-\|_{L_1}^3 \|G_+\|_{L_1}^{2k-3} + \cdots + \binom{2k}{2k-1} \|G_-\|_{L_1}^{2k-1} \|G_+\|_{L_1} \right). \end{aligned} \quad (28)$$

The above equation is just the binomial theorem with only the odd terms. By adjusting the binomial theorem to  $\frac{1}{2}((b+a)^n - (b-a)^n) = \sum_{i=1, \text{odd}}^n \binom{n}{i} a^i b^{n-i}$ , we get

$$\begin{aligned} &= \sum_{k=0}^{\infty} \frac{(\beta)^{2k+1}}{(2k+1)!} \left( (\|G_+\|_{L_1} + \|G_-\|_{L_1})^{2k+1} - (\|G_+\|_{L_1} - \|G_-\|_{L_1})^{2k+1} \right) \\ &+ \sum_{k=0}^{\infty} \frac{(\beta)^{2k}}{(2k)!} \left( (\|G_+\|_{L_1} + \|G_-\|_{L_1})^{2k} - (\|G_+\|_{L_1} - \|G_-\|_{L_1})^{2k} \right). \end{aligned} \quad (29)$$

At this point, one finds that the power series in Eq. (29) contains either odd or even terms, which fit the definitions for the hyperbolic sine and cosine functions,

$$\begin{aligned} &= \sinh(\beta(\|G_+\|_{L_1} + \|G_-\|_{L_1})) - \sinh(\beta(\|G_+\|_{L_1} - \|G_-\|_{L_1})) + \cosh(\beta(\|G_+\|_{L_1} + \|G_-\|_{L_1})) - \cosh(\beta(\|G_+\|_{L_1} - \|G_-\|_{L_1})) \\ &= 2\exp(\beta\|G_+\|_{L_1})\sinh(\beta\|G_-\|_{L_1}) \\ &= 2\exp(\beta\|\alpha I - H_-\|_{L_1})\sinh(\beta\|H_+\|_{L_1}). \end{aligned} \quad (30)$$

The bound for the NSI formula in Eq. (30) indicates that the sign problem will become exponentially severe as the off-diagonal terms in the Hamiltonian increase. However, when  $\|H_+\|_{L_1}$  reduces to precisely zero, the sign problem disappears, which meets what one would expect for stoquastic Hamiltonian. Our bound for the NSI directly links the sign problem's severity with the off-diagonal terms in the Hamiltonian.

The message we learn from the NSI formula is that a similar transformation should decrease the absolute value for both positive and negative off-diagonal elements simultaneously to mitigate the sign problem.

### Non-Stoquasticity Indicator For Complex Hamiltonians

More generally, we consider the situation where the Hamiltonian  $H$  is spanned by a complex space, the analysis becomes more complicated. Note that this is the case in the following discussion about the Hubbard model as the HVA algorithms contain complex amplitudes. The NSI by definition is the difference between the partition function of the Hamiltonian  $H$  and its Bosonic form Hamiltonian  $\tilde{H}$ . Importantly, the diagonal terms of the Hamiltonian should be real in any basis, because they correspond to the energy  $E_i = \langle \phi_i | H | \phi_i \rangle$  so that  $\alpha = \max_i H_{ii}$  is also a real number. To keep the NSI a real measure, we apply modulus to each trace for expansion of the exponential function, which gives us

$$S(H)/e^{-\beta\alpha} = \sum_{k=0}^{\infty} \frac{(\beta)^k}{k!} \text{Tr}(\tilde{G}^k) - \sum_{k=0}^{\infty} \frac{(\beta)^k}{k!} |\text{Tr}(G^k)|. \quad (31)$$



We again expand the trace in the path integral form

$$= \sum_{k=0}^{\infty} \frac{(\beta)^k}{k!} \sum_{\{\phi_i, \forall i\}} \langle \phi_0 | \tilde{G} | \phi_1 \rangle \langle \phi_1 | \tilde{G} | \phi_2 \rangle \cdots \langle \phi_{k-1} | \tilde{G} | \phi_0 \rangle - \sum_{k=0}^{\infty} \frac{(\beta)^k}{k!} \left| \sum_{\{\phi_i, \forall i\}} \langle \phi_0 | G | \phi_1 \rangle \langle \phi_1 | G | \phi_2 \rangle \cdots \langle \phi_{k-1} | G | \phi_0 \rangle \right|. \quad (32)$$

We separate the phase factor from the modulus of  $H$  for each element in the matrix,  $G = |G| \circ P(G)$ , where the  $\circ$  and  $P(G)$  denote element-wise multiplication and the phase factor matrix for  $H$ , respectively. We have

$$= \sum_{k=0}^{\infty} \frac{(\beta)^k}{k!} \sum_{\{\phi_i, \forall i\}} \tilde{G}_{0,1} \tilde{G}_{1,2} \cdots \tilde{G}_{k-1,0} \cdot P_{0,1}(\tilde{G}) P_{1,2}(\tilde{G}) \cdots P_{k-1,0}(\tilde{G}) - \sum_{k=0}^{\infty} \frac{(\beta)^k}{k!} \left| \sum_{\{\phi_i, \forall i\}} |G_{0,1}| |G_{1,2}| \cdots |G_{k-1,0}| \cdot P_{0,1}(G) P_{1,2}(G) \cdots P_{k-1,0}(G) \right|, \quad (33)$$

where we denote the  $i$ -th row,  $j$ -th column element in matrix  $X$  as  $X_{i,j}$ . Note that every nonzero element in  $P(\tilde{G})$  equals 1 in Eq. (33), so we can omit this term. Note also that  $\tilde{G}$  equals to  $|G|$  so that

$$= \sum_{k=0}^{\infty} \frac{(\beta)^k}{k!} \sum_{\{\phi_i, \forall i\}} \tilde{G}_{0,1} \tilde{G}_{1,2} \cdots \tilde{G}_{k-1,0} - \sum_{k=0}^{\infty} \frac{(\beta)^k}{k!} \left| \sum_{\{\phi_i, \forall i\}} \tilde{G}_{0,1} \tilde{G}_{1,2} \cdots \tilde{G}_{k-1,0} \cdot P_{0,1}(G) P_{1,2}(G) \cdots P_{k-1,0}(G) \right| \quad (34)$$

$$= \sum_{k=0}^{\infty} \frac{(\beta)^k}{k!} \left( \sum_{\{\phi_i, \forall i\}} \tilde{G}_{0,1} \tilde{G}_{1,2} \cdots \tilde{G}_{k-1,0} - \left| \sum_{\{\phi_i, \forall i\}} \tilde{G}_{0,1} \tilde{G}_{1,2} \cdots \tilde{G}_{k-1,0} \cdot P_{0,1}(G) P_{1,2}(G) \cdots P_{k-1,0}(G) \right| \right).$$

Notably, the last summation in Eq. (34) involves complex terms that would cancel each out. We loose this condition and attain the upper bound

$$\leq \sum_{k=0}^{\infty} \frac{(\beta)^k}{k!} \sum_{\{\phi_i, \forall i\}} \tilde{G}_{0,1} \tilde{G}_{1,2} \cdots \tilde{G}_{k-1,0} |1 - P_{0,1}(G) P_{1,2}(G) \cdots P_{k-1,0}(G)|. \quad (35)$$

In the next step, we relax the bound by decoupling the product of  $\tilde{G}_{i,j}$  from the modulus term. Also, because all non-zero terms in  $\tilde{G}$  are positive, we also apply bounds for its products of elements following the same deduction as Eq. (27). We have

$$\leq \sum_{k=0}^{\infty} \frac{(\beta)^k}{k!} \|G\|_{L_1}^k \sum_{\{\phi_i, \forall i\}} |1 - P_{0,1}(G) P_{1,2}(G) \cdots P_{k-1,0}(G)|. \quad (36)$$

Now, let us consider two arbitrary phase factors  $p_i = e^{i\theta_i}$  and  $p_j = e^{i\theta_j}$ . We can establish the triangle inequality  $|1 - p_i p_j| \leq |1 - p_i| + |1 - p_j|$ . By applying the inequality iteratively to the last modulus part of Eq. (36), we extract one phase factor out each time from the product. The resultant formula is

$$\leq \sum_{k=0}^{\infty} \frac{(\beta)^k}{k!} \|G\|_{L_1}^k \sum_{\{\phi_i, \forall i\}} \left( \sum_{r=0}^{k-1} |1 - P_{r,r+1}(G)| \right) \quad (37)$$

$$= \sum_{k=0}^{\infty} \frac{(\beta)^k}{k!} \|G\|_{L_1}^k \sum_{r=0}^{k-1} \left( \sum_{\{\phi_i, \forall i\}} |1 - P_{r,r+1}(G)| \right),$$

where we have implicitly prescribed that the next term for  $k-1$  is 0. In the second line of Eq (37), we also exchange the last two summations. By doing so, one finds that the summation runs over all possible elements for two independent basis sets  $\{|\phi_r\rangle\}$  and  $\{|\phi_{r+1}\rangle\}$ . Then, it is obvious that the outside summation will get  $k$  equal results. We get

$$= \sum_{k=0}^{\infty} \frac{(\beta)^k}{k!} \|G\|_{L_1}^k \cdot k \left( \sum_{r,l} |1 - P_{r,l}(G)| \right). \quad (38)$$

Because the two basis sets index  $\{|\phi_r\rangle\}$  and  $\{|\phi_{r+1}\rangle\}$  are independent, we change the indices to  $r$  and  $l$ . We note that all non-zero elements in the  $\tilde{G}$  matrix have phase factor 1. Thus, we change the element-wise subtraction in Eq. (38) to matrix-wise subtraction in the form of the phase matrix  $P$  and obtain

$$\begin{aligned} &= \beta \|G\|_{L_1} \|P(\tilde{G}) - P(G)\|_{L_1} \sum_{k=0}^{\infty} \frac{(\beta)^k}{k!} \|G\|_{L_1}^k \\ &= \beta \|G\|_{L_1} \|P(\tilde{G}) - P(G)\|_{L_1} \exp(\beta \|G\|_{L_1}). \end{aligned} \quad (39)$$

It is worth noting that Eq. (39) states that the sign problem relates to the norm of the Hamiltonian and also its phases of off-diagonal terms. As all phase factors of elements in  $G$  approximate 1, the sign problem alleviates. Equivalently, the more the Hamiltonian  $H$  is closer to its stoquastic counterpart  $\tilde{H}$ , the more the sign problem is relieved.

### Initial-State-Related Non-Stoquasticity Indicator

For our setting, it is particularly intriguing to investigate to what extent the quality of the initial state influences the sign problem. By quality, we mean the fidelity of the initial state compared to the ground state. For projector QMC algorithms, as we sum up the walkers at the final step, the overall stochastic implementation of the ITE process is equivalent to the following formula,

$$\frac{e^{-\beta H} |\zeta_0\rangle}{\langle \zeta_0 | e^{-\beta H} |\zeta_0\rangle}. \quad (40)$$

Here,  $|\zeta_i\rangle$  is the  $i$ -th Fock state, and the  $|\zeta_0\rangle$  is the Hartree Fock state, which is usually chosen to be the initial state for various kinds of projector QMC algorithms [18, 19].

Evidently, the partition function in Eq. (40) is related to the initial state and the basis we choose. Following the above initial-state-agnostic analysis for the partition function, here we discuss bounds for NSI equation related to the initial state. For our cases, we consider the setting that the initial state to be the VQE-optimized state  $|\psi_0\rangle = U(\vec{\theta}) |\zeta_0\rangle$ . That is we are interested in the phenomenon that when the VQE-prepared state approaches the ground state, how does the NSI behave? The main difference of the partition function from the above analysis is that the begins and ends of path integrals are restricted to the initial state  $|\psi_0\rangle$ . When the expression of Hamiltonian  $H$  is real in the basis  $\{\phi_i\}$ , the deduction of the NSI is similar to Eq. (26). We have

$$\begin{aligned} S(H, \psi_0) / e^{-\beta \alpha} &= \frac{\langle \psi_0 | e^{-\beta \tilde{H}} |\psi_0\rangle - \langle \psi_0 | e^{-\beta H} |\psi_0\rangle}{e^{-\beta \alpha}} \\ &= \sum_{k=0}^{\infty} \frac{\beta^k}{k!} \sum_{\{\phi\}} (|\langle \psi_0 | G | \phi_1\rangle \langle \phi_1 | G | \phi_2\rangle \cdots \langle \phi_{k-1} | G | \psi_0\rangle| - \langle \psi_0 | G | \phi_1\rangle \langle \phi_1 | G | \phi_2\rangle \cdots \langle \phi_{k-1} | G | \psi_0\rangle) \end{aligned} \quad (41)$$

It is not too hard to conceive that as the fidelity of the VQE-prepared state goes up, the off-diagonal terms in the 0th row of matrix  $G$ ,  $G(0)$ , will be suppressed, and become zeros when it reaches the ground state. To study the relationship between the fidelity  $|\psi_0\rangle$  and bound for the NSI, we consider the case that the second line in Eq. (41) contains  $(l-1)$ -degree of  $G(0,0)$  from the beginning, and  $(r-1)$ -degree of  $G(0,0)$  from the end of the path integral. Here, we denote  $G(0,0)$  as the 0-th row and column term in  $G$ . We sum over all possible  $l$  and  $r$ . There are two cases where negative paths involve, which are: i) a negative intermediate path both ends either both positive or negative; ii) a positive intermediate path with one end positive and the other negative. This gives us

$$\begin{aligned} &\leq 2 \sum_{k=0}^{\infty} \frac{(\beta)^k}{k!} \left( \sum_{0 \leq l < r \leq k-1} G(0,0)^{l-1+k-r} \left( \sum_{w,x,y,z=1}^{k-1} (G(0,w)_+ \cdot G(0,x)_+ + G(0,y)_- \cdot G(0,z)_-) \right. \right. \\ &\quad \cdot \sum_{\{\eta_1, \eta_2\}} \left| G_-^{(1)}(\eta_1|\eta_2) G_+^{(r-l-2)}(\eta_2|\eta_1) + G_-^{(3)}(\eta_1|\eta_2) G_+^{(r-l-4)}(\eta_2|\eta_1) + \cdots \right| \\ &\quad \left. + \binom{2}{1} \sum_{x,y=1}^{n-1} G(0,x)_+ \cdot |G(0,y)_-| \cdot \sum_{\{\eta_1, \eta_2\}} (G_+^{(r-l-1)}(\eta_1|\eta_1) + G_+^{(r-l-3)}(\eta_1|\eta_2) G_-^{(2)}(\eta_2|\eta_1) + \cdots) \right) + G(0,0)^{k-1} \sum_{x=1}^{n-1} |G(0,x)_-|, \end{aligned} \quad (42)$$

where we denote the  $i$ -th row,  $j$ -th column element of  $G$  as  $G(i, j)$ . With the same claim as Eq. (27), we have

$$\begin{aligned} &\leq \sum_{k=0}^{\infty} \frac{(\beta)^k}{k!} \left( \sum_{0 \leq l < r \leq k-1} G(0, 0)^{l-1+k-r} \left( (\|G(0, \setminus 0)_+\|_{L_1} \cdot \|G(0, 0)_+\|_{L_1} + \|G(0, \setminus 0)_-\|_{L_1} \cdot \|G(0, \setminus 0)_-\|_{L_1}) \right. \right. \\ &\quad \cdot \left. \left( (\|G_+\|_{L_1} + \|G_-\|_{L_1})^{r-l-1} - (\|G_+\|_{L_1} - \|G_-\|_{L_1})^{r-l-1} \right) \right. \\ &\quad \left. + 2\|G(0, \setminus 0)_+\|_{L_1} \cdot \|G(0, \setminus 0)_-\|_{L_1} \cdot \left( (\|G_+\|_{L_1} + \|G_-\|_{L_1})^{r-l-1} + (\|G_+\|_{L_1} - \|G_-\|_{L_1})^{r-l-1} \right) \right) \\ &\quad \left. + 2 \binom{k-1}{1} G(0, 0)^{k-1} \|G(0, \setminus 0)_-\|_{L_1} \right). \end{aligned} \quad (43)$$

Here,  $G(i, \setminus j)$  denotes the set of elements of  $G$  in row  $i$  and columns other than  $j$ . To proceed, we rearrange the terms in Eq. (43), and complete two squares

$$\begin{aligned} &= \sum_{k=0}^{\infty} \frac{(\beta)^k}{k!} \left( \sum_{0 \leq l < r \leq k-1} G(0, 0)^{l-1+k-r} \left( (\|G(0, \setminus 0)_+\|_{L_1} + \|G(0, \setminus 0)_-\|_{L_1})^2 \cdot (\|G_+\|_{L_1} + \|G_-\|_{L_1})^{r-l-1} \right. \right. \\ &\quad \left. \left. - (\|G(0, \setminus 0)_+\|_{L_1} - \|G(0, \setminus 0)_-\|_{L_1})^2 \cdot (\|G_+\|_{L_1} - \|G_-\|_{L_1})^{r-l-1} \right) + 2(k-1)G(0, 0)^{k-1} \|G(0, \setminus 0)_-\|_{L_1} \right). \end{aligned} \quad (44)$$

Next, we substitute  $r - l$  to  $\Delta$ , and Eq. (44) becomes

$$\begin{aligned} &= \sum_{k=0}^{\infty} \frac{(\beta)^k}{k!} \left( \sum_{1 \leq \Delta \leq k-1} G(0, 0)^{k-1-\Delta} \left( \binom{k-\Delta}{1} \cdot (\|G(0, \setminus 0)_+\|_{L_1} + \|G(0, \setminus 0)_-\|_{L_1})^2 \cdot (\|G_+\|_{L_1} + \|G_-\|_{L_1})^{\Delta-1} \right. \right. \\ &\quad \left. \left. - \binom{k-\Delta}{1} \cdot (\|G(0, \setminus 0)_+\|_{L_1} - \|G(0, \setminus 0)_-\|_{L_1})^2 \cdot (\|G_+\|_{L_1} - \|G_-\|_{L_1})^{\Delta-1} \right) + 2(k-1)G(0, 0)^{k-1} \|G(0, \setminus 0)_-\|_{L_1} \right). \end{aligned} \quad (45)$$

We use the gradient trick to the  $G(0, 0)$  terms in Eq. (45) to get rid of the binomial coefficient  $\binom{k-\Delta}{1}$ , and this gives us

$$\begin{aligned} &= \sum_{k=0}^{\infty} \frac{(\beta)^k}{k!} \left( \sum_{1 \leq \Delta \leq k-1} \frac{dG(0, 0)^{k-\Delta}}{dG(0, 0)} \left( (\|G(0, \setminus 0)_+\|_{L_1} + \|G(0, \setminus 0)_-\|_{L_1})^2 \cdot (\|G_+\|_{L_1} + \|G_-\|_{L_1})^{\Delta-1} \right. \right. \\ &\quad \left. \left. - (\|G(0, \setminus 0)_+\|_{L_1} - \|G(0, \setminus 0)_-\|_{L_1})^2 \cdot (\|G_+\|_{L_1} - \|G_-\|_{L_1})^{\Delta-1} \right) \right) \\ &\quad + 2\beta \|G(0, \setminus 0)_-\|_{L_1} \sum_{k=1}^{\infty} \frac{(\beta)^{k-1}}{(k-1)!} G(0, 0)^{k-1} - \frac{2\|G(0, \setminus 0)_-\|_{L_1}}{G(0, 0)} \sum_{k=0}^{\infty} \frac{(\beta)^k}{k!} G(0, 0)^k. \end{aligned} \quad (46)$$

We first compute the last term in Eq. (46)

$$\begin{aligned} &= \sum_{k=0}^{\infty} \frac{(\beta)^k}{k!} \left( \frac{d}{dG(0, 0)} \sum_{1 \leq \Delta \leq k-1} G(0, 0)^{k-\Delta} \left( (\|G(0, \setminus 0)_+\|_{L_1} + \|G(0, \setminus 0)_-\|_{L_1})^2 \cdot (\|G_+\|_{L_1} + \|G_-\|_{L_1})^{\Delta-1} \right. \right. \\ &\quad \left. \left. - (\|G(0, \setminus 0)_+\|_{L_1} - \|G(0, \setminus 0)_-\|_{L_1})^2 \cdot (\|G_+\|_{L_1} - \|G_-\|_{L_1})^{\Delta-1} \right) \right) + 2\|G(0, \setminus 0)_-\|_{L_1} \cdot \frac{2\beta G(0, 0) - 1}{G(0, 0)} \exp(\beta G(0, 0)). \end{aligned} \quad (47)$$

Note that the summation for  $\Delta$  in Eq. (47) is nothing but two geometric progressions. Applying the summation formula of geometric progression, we acquire

$$\begin{aligned} &= \sum_{k=0}^{\infty} \frac{(\beta)^k}{k!} \frac{d}{dG(0, 0)} \left( (\|G(0, \setminus 0)_+\|_{L_1} + \|G(0, \setminus 0)_-\|_{L_1})^2 \cdot \frac{G(0, 0)^k - G(0, 0)(\|G_+\|_{L_1} + \|G_-\|_{L_1})^{k-1}}{G(0, 0) - (\|G_+\|_{L_1} + \|G_-\|_{L_1})} \right. \\ &\quad \left. + (\|G(0, \setminus 0)_+\|_{L_1} - \|G(0, \setminus 0)_-\|_{L_1})^2 \cdot \frac{G(0, 0)^k - G(0, 0)(\|G_+\|_{L_1} - \|G_-\|_{L_1})^{k-1}}{G(0, 0) - (\|G_+\|_{L_1} - \|G_-\|_{L_1})} \right) \\ &\quad + 2\|G(0, \setminus 0)_-\|_{L_1} \cdot \frac{2\beta G(0, 0) - 1}{G(0, 0)} \exp(\beta G(0, 0)) \end{aligned} \quad (48)$$

The next step is to compute the gradient, and we have

$$\begin{aligned}
&= \sum_{k=0}^{\infty} \frac{(\beta)^k}{k!} \frac{(\|G(0, \setminus 0)_+\|_{L_1} + \|G(0, \setminus 0)_-\|_{L_1})^2}{G(0, 0) - (\|G_+\|_{L_1} + \|G_-\|_{L_1})} \cdot \left( (\|G_+\|_{L_1} + \|G_-\|_{L_1})^k + \left( k - 1 - \frac{k(\|G_+\|_{L_1} + \|G_-\|_{L_1})}{G(0, 0)} \right) G(0, 0)^k \right) \\
&\quad - \frac{(\|G(0, \setminus 0)_+\|_{L_1} - \|G(0, \setminus 0)_-\|_{L_1})^2}{G(0, 0) - (\|G_+\|_{L_1} - \|G_-\|_{L_1})} \cdot \left( (\|G_+\|_{L_1} - \|G_-\|_{L_1})^k + \left( k - 1 - \frac{k(\|G_+\|_{L_1} - \|G_-\|_{L_1})}{G(0, 0)} \right) G(0, 0)^k \right) \\
&\quad + 2\|G(0, \setminus 0)_-\|_{L_1} \cdot \frac{2\beta G(0, 0) - 1}{G(0, 0)} \exp(\beta G(0, 0)).
\end{aligned} \tag{49}$$

By definition of the series expansion, we finally get

$$\begin{aligned}
&= \frac{(\|G(0, \setminus 0)_+\|_{L_1} + \|G(0, \setminus 0)_-\|_{L_1})^2}{(G(0, 0) - (\|G_+\|_{L_1} + \|G_-\|_{L_1}))^2} \exp(\beta(\|G_+\|_{L_1} + \|G_-\|_{L_1})) \\
&\quad - \frac{(\|G(0, \setminus 0)_+\|_{L_1} - \|G(0, \setminus 0)_-\|_{L_1})^2}{(G(0, 0) - (\|G_+\|_{L_1} - \|G_-\|_{L_1}))^2} \exp(\beta(\|G_+\|_{L_1} - \|G_-\|_{L_1})) \\
&\quad + \frac{(\|G(0, \setminus 0)_+\|_{L_1} + \|G(0, \setminus 0)_-\|_{L_1})^2 (\beta(G(0, 0) + \|G_+\|_{L_1} + \|G_-\|_{L_1}) - 2)}{(G(0, 0) - (\|G_+\|_{L_1} + \|G_-\|_{L_1}))^2} \exp(\beta G(0, 0)) \\
&\quad - \frac{(\|G(0, \setminus 0)_+\|_{L_1} + \|G(0, \setminus 0)_-\|_{L_1})^2 (\beta(G(0, 0) + \|G_+\|_{L_1} - \|G_-\|_{L_1}) - 2)}{(G(0, 0) - (\|G_+\|_{L_1} - \|G_-\|_{L_1}))^2} \exp(\beta G(0, 0)) \\
&\quad + 2\|G(0, \setminus 0)_-\|_{L_1} \cdot \frac{2\beta G(0, 0) - 1}{G(0, 0)} \exp(\beta G(0, 0)).
\end{aligned} \tag{50}$$

Now, it is evident from Eq. (50) that every term in the NSI is suppressed at least linearly by the off-diagonal terms in  $G(0)$ . The implication is that even if we only optimize the energy as for the VQE algorithms, we nonetheless mitigate the sign problem as off-diagonal terms vanish more and more in  $G(0)$  as the prepared state gets closer to the ground state.

Whereas the Hamiltonian is complex, we follow a similar definition of NSI as Eq. (51) for the initial state-related case

$$S(H, \psi_0)/e^{-\beta\alpha} = \sum_{k=0}^{\infty} \frac{(\beta)^k}{k!} \langle \psi_0 | e^{-\beta\tilde{G}} | \psi_0 \rangle - \sum_{k=0}^{\infty} \frac{(\beta)^k}{k!} \left| \langle \psi_0 | e^{-\beta\tilde{H}} | \psi_0 \rangle \right|. \tag{51}$$

Compared to cases where the Hamiltonians are real, the formula is different from Eq. (42) in that the paths other than  $G(0, 0)$  consist of complex elements. Thus, we can simply follow the deduction in the initial-state-agnostic situation. Following the same idea as in the real case, it is natural to expect that all terms in the bound contain terms quadratic or linear to  $\|G(0, \setminus 0)\|_{L_1}$ .

To summarize, as we discussed in subsection , during alternating the walker basis, we effectively rotate the Hamiltonian with  $U(\theta)$ . This has two-fold implications for mitigating the sign problem. First, as one suppresses the off-diagonal terms in the effective Hamiltonian  $H_T(\vec{\theta})$  the sign problem is exponentially mitigated. Second, from the initial state-related analysis, we know that the sign problem is alleviated at least linearly to  $\|\Pi_{\perp} H |\psi_0\rangle\|$  with  $\Pi_{\perp} = I - |\psi_0\rangle\langle\psi_0|$ . This instructs us that rather than approximately diagonalizing the Hamiltonian, we can seek an easier way that we only optimize our ansatz state  $|\psi_0\rangle$  towards the ground state. Compared to the diagonalization of the Hamiltonian, the latter is more near-term amenable.

## QUANTUM CIRCUIT-BASED QMC

### Motivation

Although VQE algorithms have become standard prototypes for solving ground state properties regarding quantum many-body and molecular systems in the NISQ era. Several drawbacks hinder their performance in both practical and theoretical ways:

- Due to the presence of all sorts of noises, the VQE algorithms are limited to relatively shallow quantum circuits for successful implementation even aided with quantum error mitigation approaches. Thus, the expressiveness

of VQE is restricted, so the performance could be compromised especially when dealing with strong-correlated systems.

- For their variational nature, the VQE approaches are not guaranteed to converge to the optimal solution because they can get trapped in a local minimum easily as [48] proved that the loss landscape is packed out with local minimums.
- Intrinsically, the gradients of the VQE algorithms vanish exponentially as one extends the circuit depth. These types of phenomena known as “barren plateau” [90] are found ubiquitous for any highly expressive circuits that reach 2-design over the Haar measure.

From the discussion above, we know that insights are required for one to carefully choose a suitable ansatz that is both expressive enough to include the optimal solution and not too strong to bear barren plateaus. Unfortunately, no understanding has been found for systematically building reasonable VQE circuits in generic cases. Besides, for practical concerns, most error mitigation strategies are not scalable and it is hardly possible for implementing VQE experiments to go beyond the reach of classical simulation.

To facilitate research for applying quantum algorithms to study quantum many-body systems in the NISQ era, herein we suggest combining the VQE with ITE algorithms, which are well-known approaches that guarantee to produce the ground state as we go to the long-time limit. Although the operations in the ITE approaches are not unitary, classical projector QMC methods have provided the solution to implement each evolution step in a statistical way. Therefore, each step in the whole process can be made unitary. Besides, the repeated-state-preparation feature of QMC allows shallow quantum circuits to be used in the experiment. Hence, the combination of the two cutting-edge methods enables NISQ-device-friendly implementations of our Quantum Circuit-based (QC)-QMC schemes. From another perspective, we prove and numerically demonstrate in the following session that the VQE methods are found to be helpful for easing sign problem for the QC-QMC algorithms. Thus, we expect our approaches can push the limit for studying quantum many-body and chemical problems.

### Algorithm

In this section, we describe our hybrid algorithm. Following our previous discussion on sign problem, choosing an appropriate basis helps to reduce the sign problem and single Slater determinants are rather restricted in this sense. Though being an NP-hard problem, the sign problem may be alleviated using more complicated basis sets provided by NISQ devices. In the following, we will introduce our algorithm using shallow VQE circuits to transform computational basis states (single determinant state after Jordan-Wigner encoding) into entangled walkers that are closer to the diagonal basis of the Hamiltonian, which will be adopted into the FCIQMC framework to reduce the sign problem.

Now our wavefunction is expanded in a new orthonormal basis  $\{|\phi_i\rangle\}_i$ :

$$|\psi(\tau)\rangle = \sum_i \tilde{c}_i(\tau) |\phi_i\rangle \quad (52)$$

Substituting this into Eq. (14) again and taking the first-order approximation, one obtains a set of coupled differential equations for the evolution of coefficients  $\tilde{c}_i$ s:

$$-\frac{d\tilde{c}_i(\tau)}{d\tau} = \sum_j (\widetilde{H}_{ij} - S\delta_{ij})\tilde{c}_j(\tau) \quad (53)$$

where  $\widetilde{H}_{ij}$ s are the matrix elements of  $H$  under the new basis. Here we can start the energy shift  $S$  with the VQE energy and adjusts the value in a similar way as in the classical FCIQMC setting. We generate the new basis by bringing the ground state of the mean-field Hamiltonian, i.e., the Hartree-Fock state, closer to the true ground state of the Hamiltonian. We achieve this by running a variational algorithm on a quantum device starting with the Hartree-Fock state and then obtaining an optimized circuit denoted as  $U(\vec{\theta})$ . With this circuit, we now act it on the Fock basis to form a set of new basis,  $\{|\phi_i\rangle := U(\vec{\theta})|i\rangle\}$ , whose orthogonality can be easily checked as follows:

$$\langle j|U(\vec{\theta})^\dagger U(\vec{\theta})|i\rangle = \langle j|i\rangle = \delta_{ij}, \quad (54)$$

where  $\delta$  is the Dirac delta function. These new basis states are multi-configurational, and the optimized ground state  $\{U(\vec{\theta})|HF\rangle\}$  has a bigger overlap with the exact ground state than the initial Hartree-Fock state. Given Pauli



decomposition of the Hamiltonian  $H = \sum_k h_k P_k$ , the matrix elements of the Hamiltonian  $\widetilde{H}_{ij}$  under basis  $\{|\phi_i\rangle\}$  can be estimated on a quantum processor with the circuit in Fig. 3 (a) for each  $P_k$ . With the VQE energy and the new  $\widetilde{H}_{ij}$ s under the new basis, we reformulate the FCIQMC procedure as follows for the sake of completeness and we summarize the whole workflow in Algorithm 2.

- Spawning: For each walker living in  $|\phi_i\rangle$ , spawn a child walker  $|\phi_j\rangle$  ( $j \neq i$ ) with probability  $|\widetilde{H}_{ij}| \Delta\tau$  up to a normalization constant. Moreover, if this quantity  $\widetilde{H}_{ij}$  is positive, then the child has the same sign as the parent, and the opposite sign otherwise.
- Death/cloning: If the quantity  $\widetilde{H}_{ii} - S > 0$ , then walker  $|\phi_i\rangle$  dies with probability  $(\widetilde{H}_{ii} - S) \Delta\tau$ ; and if  $\widetilde{H}_{ii} - S < 0$ , then the walker clones itself with probability  $|\widetilde{H}_{ii} - S| \Delta\tau$ .
- Annihilation: At the end of each time step, we take the signed sum of walkers at each basis vector and annihilate every pair of walkers with opposite signs.

---

**Algorithm 2** QC-FCIQMC

---

**Input:** Hamiltonian  $H$ , total evolution time  $T$ , time step  $\Delta\tau$ .

**Output:** Ground state energy estimation.

Run VQE to determine  $U$  and hence  $\{|\phi_i\rangle = U|i\rangle\}$ .

Generate  $N_0$  walkers  $|\phi_0\rangle$  and let walker set  $\mathcal{D} = \{0\}$ .

**for**  $n$  in range( $T/\Delta\tau$ ) **do**

**for**  $i$  in  $\mathcal{D}$  **do**

    Estimate  $|\widetilde{H}_{ij}|$  using the circuits in Fig. 3(b).

**for**  $j$  with nonzero  $|\widetilde{H}_{ij}|$  **do**

      ▷ Spawning step

      For each walker  $|\phi_i\rangle$ , spawn a new walker  $|\phi_j\rangle$  with probability  $\Delta\tau|\widetilde{H}_{ij}|$ .

**if** New walker  $|\phi_j\rangle$  spawned **then**

        Estimate  $\widetilde{H}_{ij}/|\widetilde{H}_{ij}|$  using the circuit in Fig. 3(a)

        Label the new walker  $|\phi_j\rangle$  with the sign of  $|\phi_i\rangle$  multiplied by  $-\widetilde{H}_{ij}/|\widetilde{H}_{ij}|$ .

        Add  $j$  to  $\mathcal{D}$ .

    Estimate  $p_i = \Delta\tau(\widetilde{H}_{ii} - S)$

**if**  $p_i < 0$  **then**

      ▷ Death/cloning step

      Clone each walker  $|\phi_i\rangle$  with probability  $|p_i|$ .

**else**

      Kill each walker  $|\phi_i\rangle$  with probability  $p_i$ .

**for**  $i$  in  $\mathcal{D}$  **do**

      ▷ Annihilation step

      Annihilate the walkers  $|\phi_i\rangle$  with opposite signs.

Output the mixed energy.

---

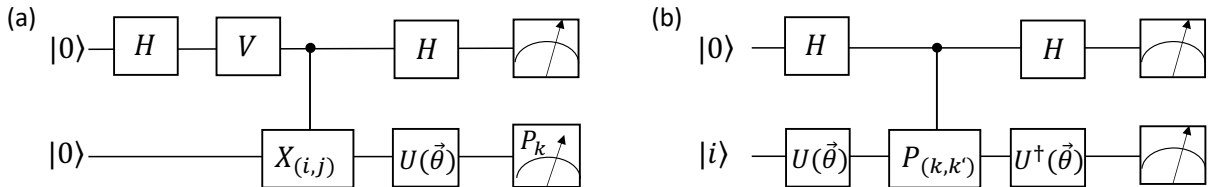


Figure 3. (a) Circuit for estimating amplitudes  $\text{Re}(\langle\phi_j|H|\phi_i\rangle)$ . One let  $V = I$  when estimating the real parts and  $V = S^\dagger = \begin{pmatrix} 1 & 0 \\ 0 & -i \end{pmatrix}$  for the imaginary parts. The gate  $X_{(i,j)}$  implements  $X_i$  if the control register is  $|0\rangle$  and  $X_j$  if the control register is  $|1\rangle$ .  $X_i$  implements  $X$  gates on those qubits where the corresponding digits in  $i$  are 1. (b) Circuit for sampling the significant amplitudes in the distribution  $|\widetilde{H}_{ij}|^2$  for a fixed  $i$ . The gate  $P_{k,k'}$  implements  $P_k$  if the control register is  $|0\rangle$  and  $P_{k'}$  if the control register is  $|1\rangle$ .

After a certain number of evolution steps, we estimate the energy by the following formula, which is similar to the FCIQMC,

$$\begin{aligned}
E(\tau) &= \frac{\langle \phi_0 | H e^{-\tau H} | \phi_0 \rangle}{\langle \phi_0 | e^{-\tau H} | \phi_0 \rangle} \\
&= E_{\text{VQE}} + \sum_{i \neq 0} \langle \phi_0 | H | \phi_i \rangle \frac{\phi_i(\tau)}{\phi_0(\tau)} \\
&= E_{\text{VQE}} + \sum_{i \neq 0} \langle \phi_0 | H | \phi_i \rangle \frac{N_i(\tau)}{N_0(\tau)},
\end{aligned} \tag{55}$$

where  $N_i(\tau)$  is the phased (signed) number of walkers  $\phi_i$  at time  $\tau$ . Though the number of possible nonzero  $\langle \phi_0 | H | \phi_i \rangle$  can be exponentially large, the total number of computing is bounded by the number of measurements of the corresponding circuit. Besides, the computing number can be further suppressed by cutting off terms with relatively small numbers of walkers compared to  $N_0$ , and still control the precision within chemical accuracy. The cutoff rate is related to the fidelity of the VQE-prepared state.

One subtlety is still left for our algorithm and we propose the solution here. The classical FCIQMC  $H_{ij}$  matrix under a single Slater determinant basis has  $\mathcal{O}(n^2\eta^2)$  non-zero elements in any one row or column because of the Slater-Condon rules, where  $n$  is the number of orbitals and  $\eta$  is the number of electrons. For our VQE basis, such polynomial bound may not be guaranteed. We use the circuit in Fig. 3 (b) to effectively sample the distribution according to  $|\widetilde{H}_{ij}|^2$ . To this end, let us re-express  $|\widetilde{H}_{ij}|^2$  as  $|\widetilde{H}_{ij}|^2 = \sum_{kk'} h_k h_{k'} p_{kk'}^i(j)$  with  $p_{kk'}^i(j) = \text{Re}\langle i | U^\dagger P_k U \Pi_j U^\dagger P_{k'} U | i \rangle$  satisfying  $\sum_j |p_{kk'}^i(j)| \leq 1$ . For given  $i, k, k'$ , we have the normalization condition  $\sum_j |p_{kk'}^i(j)| \leq 1$  and we can effectively sample according to  $p_{kk'}^i(j)$  using the quantum circuit.

Specifically, when the first register post-selects 0, the second register output configuration  $j$  with probability  $p_{k,k',+}^i(j) = \langle i | (U^\dagger P_k + P_{k'} U) \Pi_j (U^\dagger P_k + P_{k'} U) | i \rangle$ . When the first register post-selects 1, the second register output bit-string  $j$  with probability  $p_{k,k',-}^i(j) = \langle i | (U^\dagger P_k - P_{k'} U) \Pi_j (U^\dagger P_k - P_{k'} U) | i \rangle$ . One can define the following quantity thereafter

$$p_{k,k'}^i = \langle i | U^\dagger P_k U \Pi_j U^\dagger P_{k'} U | i \rangle + \langle i | U^\dagger P_{k'} U \Pi_j U^\dagger P_k U | i \rangle = \frac{p_{k,k',+}^i(j) - p_{k,k',-}^i(j)}{2}. \tag{56}$$

One can readily check that  $p_{kk'}^i(j)$  satisfies  $\sum_j |p_{kk'}^i(j)| \leq 1$  since  $\sum_j p_{k,k',+}^i(j) + p_{k,k',-}^i(j) = 1$ . And thus,  $p_{kk'}^i(j)$  can be seen as a quasi-probabilistic distribution over different  $js$  (after post-processing the outcome of the first register). To generate samples according to  $p_{kk'}^i(j)$ , one simply gets measurement results from the quantum circuit and post-process the results. According to the outcomes of the ancillary qubit, either  $|0\rangle$  or  $|1\rangle$ , we assign different signs 1 or  $-1$  to the outcomes, and then group the outcome with the same  $|j\rangle$ s together. For example, when we get  $N_{k,k',+}^i(j)$  and  $N_{k,k',-}^i(j)$  counts for outcomes  $0j$  and  $1j$ , we equivalently get  $N_{k,k',+}^i(j) - N_{k,k',-}^i(j)$  outcomes with respect to the quasi-probability  $p_{kk'}^i(j)$ . Normalizations of the samples (over the total number of samples) would thus give an unbiased estimation of the quasi-probability  $p_{kk'}^i(j)$ . According to the Hoeffding's inequality [91], the number of samples we need to estimate  $p_{kk'}^i(j)$  to accuracy  $\varepsilon$  is  $\mathcal{O}(1/\varepsilon^2)$ . Next, we repeat this sampling process to obtain samples and hence unbiased estimators of  $p_{kk'}^i(j)$  for each index  $k, k'$ . Then we get  $|\widetilde{H}_{ij}|^2$  by combining the results according to  $|\widetilde{H}_{ij}|^2 = \sum_{kk'} h_k h_{k'} p_{kk'}^i(j)$ . The empirical estimation of the distribution  $|\widetilde{H}_{ij}|^2$  converge to its ideal value rapidly by Bernstein bound. We analyze the sufficient number of samples in Sec. .

In order to increase the efficiency of this sampling procedure, one can choose only to sample the  $(k, k')$  pairs whose factors  $h_k h_{k'}$  are above a certain threshold. Meanwhile, one can adjust the number of  $j$  samples for a specific  $p_{k,k'}^i$  to be proportional to its factor  $h_k h_{k'}$ , such that the  $js$  that contributes more to  $|\widetilde{H}_{ij}|^2$  is more likely to be selected and sampling efficiency is thus improved.

### Complexity Analysis

In this section, we estimate the total time complexity of our algorithm. This can be divided into two parts, which are the complexity using Fig. 3 (a) to sample the entries in the Hamiltonian matrix for estimation; and the estimation of these entries using Fig. 3 (b). The rest is classical post-processing just like classical FCIQMC.

Now we first estimate the number of non-negligible matrix elements "connected" to a given configuration, where "connected" means the set of walkers  $|\{j\}|$  that is of non-zero  $\langle j | H | i \rangle$  for a given configuration  $i$ . Without loss

generality, we take molecular systems as instances in this section. In the original setting of the classical FCIQMC, the sampling procedure at each step is promised to be efficient in that the “connected” number of walkers  $|\{j\}|$  for a given walker  $|i\rangle$  is at most polynomial to the system size. This is because the allowed non-zero walkers  $|j\rangle$  for  $\langle j|H|i\rangle$  those differ from  $|i\rangle$  by at most four sites in the Fock space for two-body terms are the most non-local terms in  $H$ . The space for the “connected” walkers  $\{j\}$  is thus of size  $\mathcal{O}(n^4)$  for molecular systems, and so the sufficient sampling number are bounded to a polynomial of  $n$ . However, this is not the case for our QC-FCIQMC method as the size of the non-zero  $|\{j\}|$  is of order  $\mathcal{O}(\exp(n))$ . This can be seen by performing the Baker–Campbell–Hausdorff (BCH) formula to the ansatz  $U(\vec{\theta})$ . However, we show in the following that the number of walkers with coefficients above a certain threshold is at most polynomial to  $n$  as long as the required threshold  $\epsilon$  is a constant. To explain this, let us consider the ansatz in the following form,

$$U(\vec{\theta}) = \prod_{j=1}^N \exp(-i\theta_j T_j), \quad (57)$$

where each  $T_i$  is an operator that satisfies  $T_i^2 = \mathbb{1}$ , e.g., the Pauli operators; and  $N$  is the total number of gates compiled into the exponential form. Note that any elements from the SU group can be compiled into this form, and thus Eq. (57) serves as a generic strategy for implementing arbitrary ansatz. For instance, the UCCSD ansatz is compiled into the form of Eq. (57) by applying the Jordan-Wigner transformation and the Trotter formula [83]. In the following, we estimate the size of the operator space  $\mathcal{S}_\epsilon(U(\vec{\theta})^\dagger H U(\vec{\theta}))$ , which is the set of operators with the absolute value of coefficients no less than  $\epsilon$ . Given the form of the compiled ansatz in Eq. (57), Ref. [92] gives the exact formula of the transformed Hamiltonian in the following iterative form

$$\begin{aligned} H_{(k)}(\theta_k, \dots, \theta_1) &= \exp(i\theta_k T_k) H_{(k-1)}(\theta_{k-1}, \dots, \theta_1) \exp(-i\theta_k T_k) \\ &= \frac{1}{2}(3 - \cos \theta_k) H_{(k-1)} + \sin \theta_k \left( -\frac{i}{2} [H_{(k-1)}, T_k] \right) + \frac{1}{2}(1 - \cos \theta_k) T_k H_{(k-1)} T_k, \end{aligned} \quad (58)$$

where  $H_{(k)}$  is the Hamiltonian after  $k$ -th step of iteration, and there are total  $N$  iteration for  $U(\vec{\theta})^\dagger H U(\vec{\theta})$ . After each iteration, the total number of operators becomes 3-fold comparing to the one from previous step. Hence, the size of operator space grows in a  $3^N$  fashion relative to the number of operators in  $H$ , that is  $\mathcal{O}(n^4)$ . Note that from the second line of Eq. (58), only the second and third terms will introduce new operators compared to  $H_{(k-1)}$ . To evaluate the size of  $\mathcal{S}_\epsilon(U(\vec{\theta})^\dagger H U(\vec{\theta}))$ , we let the following two equations hold

$$\left\{ \begin{array}{l} \left| \prod_{j=1}^m -\frac{i}{2} \sin \theta_j \right| = \epsilon, \\ \left| \prod_{j=1}^m \frac{1}{2} (1 - \cos \theta_j) \right| = \epsilon. \end{array} \right. \quad (59)$$

It is found that when  $m = \mathcal{O}(\log \frac{1}{\epsilon})$ , the absolute value of coefficients of newly introduced operators in Eq. (57) are no more than  $\epsilon$  by letting each  $\sin \theta_j$  and  $\cos \theta_j$  in Eq.(59) equals to one. It follows that  $|\mathcal{S}_\epsilon(U(\vec{\theta})^\dagger H U(\vec{\theta}))|$  is of size  $\left(1 + \binom{N}{1}(2+1) + \binom{N}{2}(2+1)^2 + \dots + \binom{N}{m}(2+1)^m\right) = N^{\mathcal{O}(m)}$ -fold of the operators in  $H$ . Here, the  $(2+1)$  in the formula follows from the second ( $[H_{(k-1)}, T_k]$ ) and third term ( $T_k H_{(k-1)} T_k$ ) in the second line of Eq. (57) that the two terms will introduce at most 2- and 1-fold of new operators comparing to that of  $H_{(k-1)}$ , respectively. In summary, the size of operator space  $\mathcal{S}_\epsilon(U(\vec{\theta})^\dagger H U(\vec{\theta}))$  is  $N^{\mathcal{O}(\log(1/\epsilon))} n^4$ .

In the above discussion, we provide evidence that the number of non-negligible terms (i.e., terms with coefficients above a certain threshold in magnitude) grows in a polynomial way with the system size. However, the brutal-force cutoff of other negligible terms will introduce bias to the ITE process. This is because the number of these negligible terms is exponential, and thus their overall contribution is non-negligible. To address this problem, we invoke the sampling process introduced in Sec. that both avoids the exponentially many terms and preserves the distribution of walkers statistically as shown by Fig. 3 (b). This sampling procedure provides i.i.d. samples according to the distribution  $|\widetilde{H}_{ji}|^2 := |\langle \phi_j | H | \phi_i \rangle|^2$ . The sampling procedure allows us to effectively capture the exponentially growing space of walkers in a way that we spawn walkers according to their importance, i.e., magnitudes. The ITE process of the QC-FCIQMC method is thus unbiased.

Finally, we analyze the sufficient number of samples. As we can only afford a polynomial number of samples, the number of samples is related to the degree of cutoff for the walkers of the ITE process. As the accuracy we want to achieve is  $\epsilon$ , a sufficient number of sample  $Z$  is proportional to the size of  $\mathcal{S}_\epsilon(U(\vec{\theta})^\dagger H U(\vec{\theta}))$  that equals to  $N^{\mathcal{O}(\log(1/\epsilon))} n^4$  for each  $|\phi_i\rangle$  as analyzed in the above discussion. For our work, we use the ADAPT-VQE and HVA algorithms as ansatz, and in both cases,  $N = \mathcal{O}(n)$ . This gives the number of samples that is upper bounded by  $Z = n^{\mathcal{O}(\log(1/\epsilon))+4}$ , which is still an  $n^{\mathcal{O}(\log(1/\epsilon))}$  increment comparing to the classical FCIQMC. However, we stress that the upper bound is by no means tight as we have let  $|\prod_{j=1}^m \sin \theta_j| = |\prod_{j=1}^m (1 - \cos \theta_j)| = 1$  in Eq. (59) that in practice the sufficient number of samples can be far smaller than this estimation. We further remark that recent developments [84, 93] employ particle-number preserving gates for fermionic ansatz compilation, such as the Givens rotation gates [84]. In this way, it is often the case that the basis rotation operator ( $\exp(K)$ , where  $K = \sum_{ij} \theta_{ij} (a_i^\dagger a_j - a_j^\dagger a_i)$  is an anti-hermitian) is employed as a subroutine in the quantum circuits. The basis rotation circuit shall not increase the number of operators for the Hamiltonian, which is favorable for our QC-FCIQMC protocol. We as well use this compilation method for the single-body terms in the HVA ansatz.

As a side note to the sampling process, we also provide a method to determine if the current number of samples is sufficient or not. This can be done by resorting to an ‘‘online’’ approach that compares the probabilistic distribution of the sample by adding a small number of samples  $l$  to that without adding the  $l$  new samples. Following this idea, the sampling strategy is that one starts from a relatively small number of samples  $L$  and keeps adding  $l$  samples, and then compares if the distribution is changed or not up to some threshold. In this way, if the distribution does not change for enough rounds of sample-adding, it means the number of samples is sufficient.

In the above, we have discussed the sufficient number of samples needs to collect according to  $|\widetilde{H}_{ji}|^2 := |\langle \phi_j | H | \phi_i \rangle|^2$  and its corresponding sampling strategy. Suppose for a fixed  $i$ , we have garnered enough sample, and the walker set is denoted as  $\mathcal{D}^i = \{|\phi_j\rangle\}$ . The next step is to estimate each  $\widetilde{H}_{ji} := \langle \phi_j | H | \phi_i \rangle$  within given accuracy  $\epsilon$  for all  $|\phi_j\rangle$  in the walker set  $\mathcal{D}^i$  using quantum circuit depicted in Figure 3 (a). The sample complexity for achieving this goal is analyzed as follows.

**Lemma 3** (Sample complexity for estimating  $\widetilde{H}_{ji}$ ). *Given Hamiltonian  $H = \sum_{k=1}^K h_k P_k$  and target  $i, j$  for  $\widetilde{H}_{ij}$ , let  $\{\mathbf{A}_{ijk}^{(l)}, \mathbf{B}_{ijk}^{(l)}\}_{k,l=1}^{K, L_k}$  be  $M = \sum_{k=1}^K L_k$  samples that are measurement outcomes from quantum circuits given in Figure 3 (a) with  $V = I$  and  $S^\dagger$ , respectively, and  $i, j, k$  are set to given indices. Define  $\bar{\mathbf{C}}_{ijk}$  as*

$$\bar{\mathbf{C}}_{ijk} := \frac{1}{L_k} \sum_{l=1}^{L_k} h_k (\mathbf{A}_{ijk}^{(l)} + i \mathbf{B}_{ijk}^{(l)}). \quad (60)$$

Then, the estimator for  $\widetilde{H}_{ji}$  defines as

$$\bar{\mathbf{C}}_{ij} := \sum_{k=1}^K \bar{\mathbf{C}}_{ijk}. \quad (61)$$

Also, define  $h_s := \sum_{k=1}^K |h_k|$ . Then for any  $\epsilon > 0$  and  $\mu \in (0, 1)$ , let each  $L_k$  takes the following value

$$L_k := \left\lceil \frac{|h_k|^2 \ln(4K/\mu)}{\epsilon_k^2} \right\rceil, \quad (62)$$

where  $\epsilon_k$  is given by

$$\epsilon_k^2 := \frac{|h_k|}{h_s} \epsilon^2. \quad (63)$$

Then, when the total number of samples  $M$  gives by

$$M := \left\lceil \frac{h_s^2 \ln(4K/\mu)}{\epsilon^2} \right\rceil, \quad (64)$$

we have

$$\mathbb{P} \left[ |\bar{\mathbf{C}}_{ij} - \widetilde{H}_{ji}| < \epsilon \right] \geq 1 - \mu. \quad (65)$$

*Proof.* Note that Eq. (61) serves as an unbiased estimator for evaluating the  $h_k \langle \phi_j | P_k | \phi_i \rangle$ , such that  $\mathbb{E}[\bar{\mathbf{C}}_{ijk}] \equiv h_k \langle \phi_j | P_k | \phi_i \rangle$ . Therefore, Eq. (61) serves as an unbiased estimator for estimating the  $\widetilde{H}_{ji}$ , and the empirical mean value approaches the expectation value when more samples are collected. For each  $k \in [1, K]$ , the value of  $\text{Re}(\bar{\mathbf{C}}_{ijk})$  and  $\text{Im}(\bar{\mathbf{C}}_{ijk})$  are in  $[-|h_k|, |h_k|]$  as  $\mathbf{A}_{ijk}^{(l)}$  and  $\mathbf{B}_{ijk}^{(l)}$  take value in  $[-1, 1]$ . When taking the number of samples as Eq. (62) for all  $k \in [1, K]$ , the following formulas hold by applying Hoeffding's inequality [91],

$$\begin{cases} \mathbb{P} \left[ \left| \text{Re}(\bar{\mathbf{C}}_{ijk}) - \text{Re}(h_k \langle \phi_j | P_k | \phi_i \rangle) \right| > \frac{\epsilon_k}{\sqrt{2}} \right] < \frac{\mu}{2K}, \\ \mathbb{P} \left[ \left| \text{Im}(\bar{\mathbf{C}}_{ijk}) - \text{Im}(h_k \langle \phi_j | P_k | \phi_i \rangle) \right| > \frac{\epsilon_k}{\sqrt{2}} \right] < \frac{\mu}{2K}. \end{cases} \quad (66)$$

By applying the triangle inequality and the union bound of the above two formulas, we have

$$\mathbb{P} \left[ \left| \bar{\mathbf{C}}_{ijk} - h_k \langle \phi_j | P_k | \phi_i \rangle \right| > \epsilon_k \right] < \frac{\mu}{K}. \quad (67)$$

Finally, when choosing each  $\epsilon_k$  as Eq. (63), the overall  $\epsilon$  accuracy is achieved for evaluating  $\widetilde{H}_{ji}$  by applying the union bound to all  $k \in [1, K]$ :

$$\mathbb{P} \left[ \left| \bar{\mathbf{C}}_{ij} - \widetilde{H}_{ji} \right| > \epsilon \right] < \mu. \quad (68)$$

And the total number of samples  $M$  is obtained by substituting Eq. (63) into Eq. (62)

$$\begin{aligned} M &= \sum_{k=1}^K L_k \\ &= \sum_{k=1}^K \left\lceil \frac{h_s |h_k| \ln(4K/\mu)}{\epsilon^2} \right\rceil \\ &= \left\lceil \frac{h_s^2 \ln(4K/\mu)}{\epsilon^2} \right\rceil. \end{aligned} \quad (69)$$

Note that the sample complexity is similar to that of the energy measurement process for near-term quantum devices using the frequentist approach [66, 83] as the quantity that we estimate here has a similar form to the energy.

In summary, given  $\epsilon > 0$  and  $\mu \in (0, 1)$ , the complexity of our QC-FCIQMC protocol can be summarized as follows:

1. The computational complexity for sampling according to  $|\widetilde{H}_{ji}|^2$  is given by  $N_s = (N^{\mathcal{O}(\log(1/\epsilon))} h_s^2)$  where  $N$  is defined in Eq. (57). The  $h_s^2$  is coming from the sampling strategy that we presented in the previous section, where the number of samples taken for a  $(k, k')$  pair is proportional to the amplitude of  $h_k h_{k'}$ .
2. A total  $\widetilde{\mathcal{O}}(h_s^2 \epsilon^{-2})$  number of samples needs to be collected to reach  $\epsilon$  accuracy for evaluating each  $\widetilde{H}_{ji}$  with at least  $1 - \mu$  probability, where the  $\widetilde{\mathcal{O}}$  notation have omitted poly-logarithmic scaling.
3. For the  $t$ -th round of walker set  $\mathcal{D}^{(t)}$  of size  $|\mathcal{D}^{(t)}|$ , the total time complexity for iterating to the next round  $t + 1$  is  $\widetilde{\mathcal{O}}(|\mathcal{D}^{(t)}| N_s + |\mathcal{D}^{(t)}| N'_s h_s^2 \epsilon^{-2})$ . Here,  $N'_s$  is the total number of different sampled walkers that satisfies  $N'_s \leq N_s$ . One can see that the second term dominates the scaling compared to the first term.

We stress that this number of walkers only relates to the number of samples we need to measure from the quantum circuit, but does not represent the number of walkers we finally need to store. This is because the number of walkers will be significantly suppressed after we implement the annihilation step of the QC-FQCIQMC method. Besides, note that the size of the walker set  $|\mathcal{D}^{(t)}|$  at each round is turned out to be determined by the severity of the sign problem, which could induce an exponential factor to the total time complexity. As shown theoretically in Sec. , our QC-FCIQMC approach holds the potential to mitigate the sign problem in an exponential way, which could potentially provide a quantum advantage for near-term quantum experiments as our protocol is amenable for nowadays quantum hardware. In Sec. , we validate our theoretical understanding by showing the suppression of the sign problem with a better basis obtained by the VQE algorithms using numerical techniques for both quantum chemistry and many-body systems.



### Comparison with Other Methods

In this section, we compare our method with recent states-of-the-art ground state energy estimation quantum algorithms [30, 31, 34, 94, 95] in a computational complexity sense in the following.

Recently, quantum algorithms [30, 31, 34, 94, 95] are designed regarding the ground state problems that allow a shorter circuit-depth comparing to quantum phase estimation methods and also achieve (near)-optimal scaling [94] in query complexity at the same time. Those quantum algorithms are designed for early-fault-tolerant quantum devices, where the decoherence time is supposed to be longer than near-term devices but is still limited. Besides, the number of logical qubits is limited; as such, it is favorable to employ as less as possible ancillary qubits. We provide the query complexity and maximal circuit-depth comparison between our method and those state-of-the-art quantum algorithms. Particularly, we focus on three specific properties of an algorithm: i) Maximal circuit depth that needs to be implemented in one round; ii) Number of ancillary qubits needed; iii) The main subroutine that determines whether or not the method needs multi-qubit-control operations. These three properties determine whether we should implement the quantum algorithm on near-term, early-fault-tolerant, or full-fledged quantum computers.

Two assumptions are made for discussion of the query complexity: i) an initial state  $\phi_0$  is known and its low bound  $\gamma$  of overlap between the initial state and the ground state is provided, such that  $|\langle \phi_0 | \Psi_0 \rangle| \geq \gamma$ , where  $|\Psi_0\rangle$  is the ground state of  $H$ ; ii) a lower bound  $\Delta$  of the energy gap between the ground and first-excited state of the Hamiltonian is given, such that  $E_1 - E_0 \geq \Delta$ , where  $E_0$  and  $E_1$  are ground and first-excited state energy of  $H$ , respectively. We summarize the main properties of each quantum algorithm in the following table. We summarize the main properties of each quantum algorithm in the following table.

Table I. Quantum algorithms performance for the ground state energy estimation problem

	maximal query/circuit depth	query complexity	number of ancillary qubits	main subroutine
QPE	$\tilde{\mathcal{O}}(\epsilon^{-1})$	$\tilde{\mathcal{O}}(\epsilon^{-1}\gamma^{-2})$	$\mathcal{O}(\text{polylog}(\gamma^{-1}\epsilon^{-1}))$	controlled Hamiltonian evolution + Quantum Fourier transform
Iterative QPE	$\tilde{\mathcal{O}}(\epsilon^{-1}\gamma^{-2})$	$\tilde{\mathcal{O}}(\epsilon^{-1}\gamma^{-4})$	$\mathcal{O}(1)$	controlled Hamiltonian evolution + Hadamard test
LT [30]	$\tilde{\mathcal{O}}(\epsilon^{-1})$	$\tilde{\mathcal{O}}(\epsilon^{-1}\gamma^{-4})$	$\mathcal{O}(1)$	controlled Hamiltonian evolution + Hadamard test
Wan <i>et al.</i> [31]	$\tilde{\mathcal{O}}(\epsilon^{-2}\lambda^2)$	$\tilde{\mathcal{O}}(\lambda^2\epsilon^{-2}\gamma^{-4})$	$\mathcal{O}(1)$	controlled Paulis + Hadamard test
Wang <i>et al.</i> [95]	$\tilde{\mathcal{O}}(\Delta^{-1})$	$\tilde{\mathcal{O}}(\epsilon^{-2}\Delta\gamma^{-4})$	$\mathcal{O}(1)$	controlled Hamiltonian evolution + Hadamard test
DLT [34]	$\tilde{\mathcal{O}}(\epsilon^{-1}\gamma^{-1})$	$\tilde{\mathcal{O}}(\epsilon^{-1}\gamma^{-1})$	$\mathcal{O}(1)$	controlled Hamiltonian evolution + quantum signal processing
This work	$\mathcal{O}(n)$	$\Omega(\epsilon^{-2}\gamma^{-4})$	$\mathcal{O}(1)$	controlled Paulis + Hadamard test

Let us analyze the table. First, the ‘‘maximal query/circuit depth’’ column decides the maximal times that one queries the ‘‘main subroutine’’ in one round of the algorithm. For example, the work of Lin and Tong [30] uses a Hadamard-test-like circuit, and it queries a controlled Hamiltonian evolution  $e^{-iHt}$  circuit at iteration, and the maximum evolution time for the Hamiltonian evolution at single iteration is  $t = \tilde{\mathcal{O}}(\epsilon^{-1})$ . Thus, it is nevertheless hard to implement these types of algorithms on near-term quantum devices. Besides, all the algorithms designed for early-fault-tolerant devices only require  $\mathcal{O}(1)$  ancillary qubits. For our work, because we do not need to query an oracle, the circuit depth other than the initial state preparation is at most  $\mathcal{O}(n)$  of controlled Paulis. This originates from that the QC-FCIQMC method needs to control each Pauli term shown in the Hamiltonian as depicted in Fig. 3 (a) and (b). Because the fermionic annihilation and generation operators are non-local, i.e., they transform to Pauli operators that support on  $\mathcal{O}(n)$  qubits, this gives the  $\mathcal{O}(n)$  scaling in our algorithm. We note that our circuit-depth requirement is suitable for near-term quantum devices according to recent experimental demonstrations of VQE methods [96–99].

We note that the work of Wan *et al.* [31] have a similar realization of our work in that they take advantage of the qDRIFT random compiler [100] for implementing the Hamiltonian evolution resulting in the controlled Paulis compilation of quantum circuits. The largest number of single-qubit controlled Pauli implement in one round of the algorithm in Ref. [31] is  $\tilde{\mathcal{O}}(\epsilon^{-2}\lambda^2)$ , where  $\lambda = \sum_k |h_k|$  for  $H = \sum_k h_k P_k$ . For quantum molecular problems, the circuit depth could be prohibitive for near-term quantum devices given the chemical accuracy,  $\epsilon = 1 * 10^{-3}$  Hartree. We also remark that although our work calls the initial state preparation unitary  $U(\vec{\theta})$  twice in Fig. 3 (b), this will not induce significant resource overhead as long as  $U(\vec{\theta})$  is near-term-achievable.

For our QC-FCIQMC method, we focus on the complexity for estimation of the ground state energy after sufficient rounds of iteration, i.e., the evolution time of ITE is large enough that  $\beta \sim \frac{1}{\Delta\gamma}$ . Because the complexity of our algorithm depends on the severity of the sign problem (which determines the final number of walkers), this makes it hard to analyze for our work. However, when the sign problem has been properly dealt with, we are able to analyze the lower bound for the complexity of our QC-FCIQMC method. That is  $\Omega(\epsilon^{-2}\gamma^{-4})$ , which implies that the total number of walkers is proportional to  $\gamma^{-4}$ . This is because the partition function (denominator of the energy estimator given by Eq. (55)) can be no larger than  $\gamma^{-2}$  at best. As such, when we analyze the sample complexity for estimation of the expectation value of an observable, the  $\gamma^{-2}$  factor is squared by using Hoeffding’s inequality [91].

In conclusion, although the total complexity of our work may not be favorably compared to other state-of-the-art fault-tolerant quantum algorithms, we manage to reduce the circuit depth to the point that is manageable for NISQ devices. We emphasize that our method is designed from a piratical perspective for near-term quantum technologies. We quantify the quantum-classical separation between QC-FCIQMC and classical QMC approaches by computing the upper bound for the NSI given by Eq. (21). As such, we can measure to what extent the sign problem is suppressed. In summary, our method is of immediate interest to experimental research; and hopefully demonstrates a practical advantage of quantum algorithms.

In the next section, we show numerically that severity of the sign problem can be significantly suppressed with even a rather shallow quantum circuit, which is near-term-amenable. Besides, as the circuit depth of the VQE increases, the upper bound for the NSI drops rapidly, indicating a systematic improvement for the sign problem.

## NUMERICAL RESULTS

In this section, we present numerical results demonstrating the effectiveness of the QC-FCIQMC algorithm at easing the sign problem and reducing the number of walkers as well as the energy variance compared to classical FCIQMC. We pick two strongly correlated systems to ensure the robustness of our scheme, the  $N_2$  molecule at the dissociation limit and the  $2 \times 4$  Hubbard model with  $U/t = 4$ .

We plot the potential energy surface of  $N_2$  molecule with our QC-FCIQMC algorithm in Fig. 4 (a). The new walker bases for all bond lengths are prepared by ADAPT-VQE circuits that add 12 fermionic operators. In Fig. 4 (b), we plot the standard deviation from energy profile along the QC-FCIQMC evolution. We freeze the 1s and 2s orbitals and run ADAPT-VQE with 12 qubits. We also plot data from a single determinant FCIQMC for comparison. We set 10000 walkers to be the threshold for both algorithms to start the energy shift. On the one hand, we see that QC-FCIQMC is able to push the results of shallow ADAPT-VQE circuits to the level of chemical accuracy across all bond lengths, therefore easing the burden on the quantum devices. Meanwhile, using the same amount of walkers, single determinant FCIQMC fails to reach chemical accuracy at some of the bond lengths towards the dissociation limit. On the other hand, the energy deviation of QC-FCIQMC is smaller than that of single determinant FCIQMC. Therefore, QC-FCIQMC would require much fewer energy evaluations to obtain a precise energy estimation and maybe smaller total evolution time. All the energy and standard deviation are evaluated by taking energies after reaching a certain total evolution time, and usually, after the total number of walkers stabilizes. We adopt this way of evaluation for all of the following numerical experiments.

For the  $N_2$  molecule at bond length  $4.0\text{\AA}$ , we use quantum circuits from ADAPT-VQE that add different numbers of operators to generate the new basis of QC-FCIQMC. We plot the effect of energy variance reduction of QC-FCIQMC given a fixed number of walkers in Fig. 4 (c) (d). The standard deviation is reduced by close to 100 folds going from a single determinant basis to ADAPT-VQE adding 24 operators. We highlight that at this depth, QC-FCIQMC achieves a standard deviation within the range of chemical accuracy with only 10000 walkers.

In Fig. 4 (e) (f), we conversely plot the total walker number required for QC-FCIQMC runs assisted by ADAPT-VQE circuits of different depths to maintain a similar level of precision. The total number of walkers decreases by two orders of magnitude going from the basis generated by ADAPT-VQE adding 4 operators to that generated by ADAPT-VQE adding 24 operators.

As we discussed in the last section, one can sample the configurations  $js$  for which one calculates the corresponding matrix elements  $H_{ijs}$  with respect to a given  $i$ . One can choose a certain threshold for the number of  $js$  given  $i$  where one stops sampling more configurations. In Fig. 5, we plot the effects of taking a limited number of samples for the selection of  $j$  configurations spawning from  $i$  in  $N_2$  simulation. We again use the VQE basis generated by 12 layers of ADAPT-VQE. We stop the sampling procedure after reaching a certain number of  $j$  configurations for each  $i$ . We adjust this threshold to obtain the five data points in the figure and one can see the fewer samples we take, the larger the deviation from the exact energy. We can also observe that the variance does not vary much with the number of

samples, which instead depends more on the number of layers of the ADAPT-VQE as shown in Fig. 4(c).

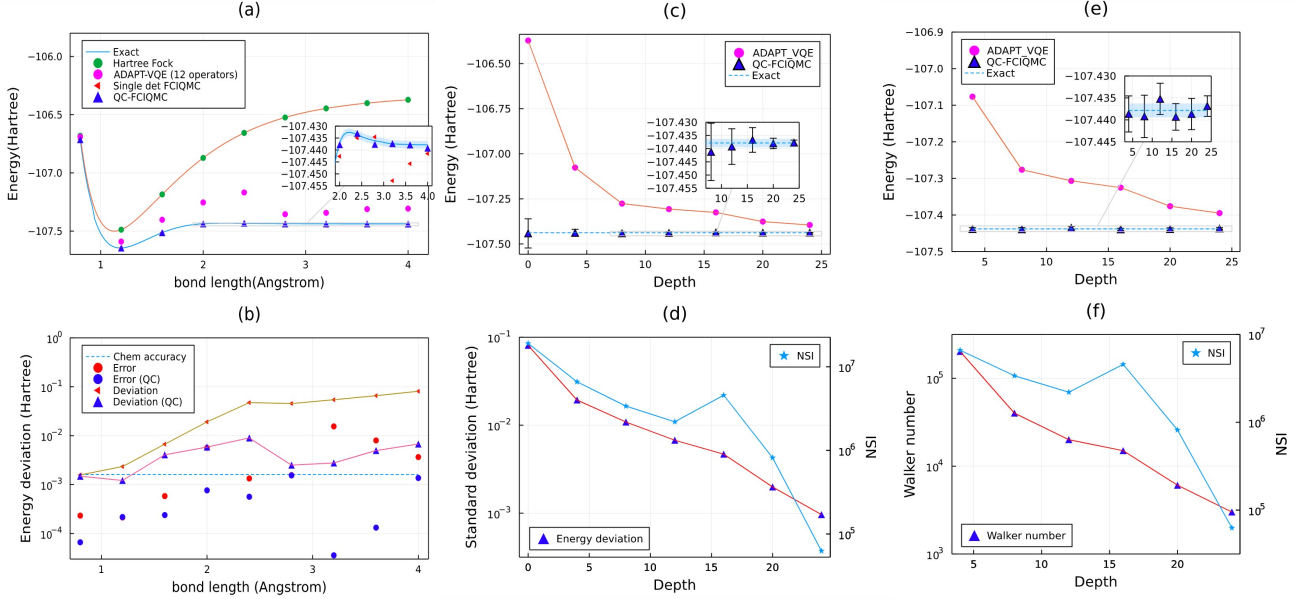


Figure 4. (a) Potential energy surface for the nitrogen molecule with QC-FCIQMC under the STO-3g basis set. (b) The standard deviation of energy evaluations along the QMC evolution. Here the new walker space of QC-FCIQMC is prepared with circuits from ADAPT-VQE (adding 12 fermionic operators for all bond lengths). Even with the assistance of shallow-depth ADAPT-VQE runs, QC-FCIQMC manages to reach chemical accuracy across all bond lengths using only around 10000 walkers. We also include data from FCIQMC with single-determinant walkers for comparison. For both single determinant FCIQMC and QC-FCIQMC, we start the energy shift when the total number of walkers exceeds 10000. Under this setting, single determinant FCIQMC fails to reach chemical accuracy at several bond lengths towards the dissociation limit. Moreover, the standard deviation from the energy profiling of QC-FCIQMC is smaller than the single determinant FCIQMC for all bond lengths. In fact, one observes a bigger variance reduction with a stronger static correlation. (c) FCIQMC-assisted ADAPT-VQE results for nitrogen molecule at bond length 4.0. ADAPT-VQE energies and QC-FCIQMC energies with standard deviations for different depths of ADAPT-VQE. (d) Log plot with standard deviations from (c) as well as the non-stoquastic indicator, where choose  $\beta = 10^{-1}$ . FCIQMC is able to push ADAPT-VQE results of different depths to chemical accuracy. Here we obtain the expected energy by taking the average of all FCIQMC energies after it converges. We fix the total walker number at the same level by starting to implement an energy shift of  $S$  when the total walker number exceeds  $10^4$ . The deeper the ADAPT-VQE circuit is, the smaller the energy variance FCIQMC would have. One can see with an ADAPT-VQE optimization that picks 20 operators, the energy variance obtained is already at a similar level as chemical accuracy requirement and with 24 operators the variance lies well within chemical accuracy area. (e) ADAPT-VQE energies and QC-FCIQMC energies with variances for different depths of ADAPT-VQE. (f) Log 10 plots of the respective numbers of walkers that give the energies in (e) as well as the natural log of the non-stoquastic indicator, where choose  $\beta = 10^{-1}$ . To reach a certain level of energy variance, FCIQMC requires fewer walkers assisted with deeper ADAPT-VQE circuits. Here we choose the energy variance upper bound to be 5mHa for the number of walkers to be friendly to the running time of our code. To reach this precision, QC-FCIQMC requires about 100 times fewer walkers going from ADAPT-VQE with 4 operators to that of 24 operators.

We also test our QC-FCIQMC algorithm on the Hubbard model. Here we choose the Hubbard model of size 2, which requires 16 qubits and pick  $U/t = 4$  to enable stronger static correlation. We also choose the chemical potential as half-filling. In Fig. 6, we compare the performance of QC-FCIQMC with the basis generated from the Hamiltonian variational ansatz (HV ansatz) [66–68] and the classical FCIQMC with single determinant basis. With the basis generated by a 15-layer HV ansatz, we observe the fluctuations of the energy much smaller in (a) and the walker population much more concentrated on a few configurations in (c) than the single-determinant basis in (b). We also plot the suppression of energy variance for HV ansatz with 1, 5, 10, and 15 layers in Fig. 6 (d) (e). We remark that the standard deviation of energy evaluation is reduced by almost one order of magnitude with merely a 1-layer HV ansatz.

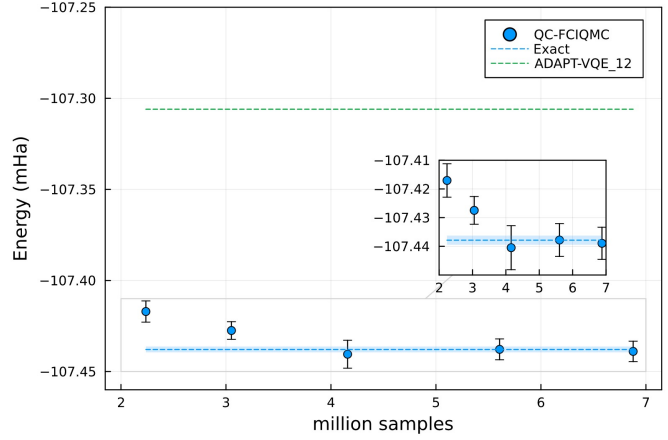


Figure 5. QC-FCIQMC on  $N_2$  molecule at bond length  $4.0\text{\AA}$  when taking limited number of samples for the selection of  $j$  configurations spawning from  $i$ . Here we use the VQE basis generated by 12 layers of ADAPT-VQE and the  $x$ -axis denotes the total number of samples of the whole QMC process. One can see the fewer samples we take, the larger the deviation from the exact energy. We can also observe that the variance does not vary much with the number of samples.

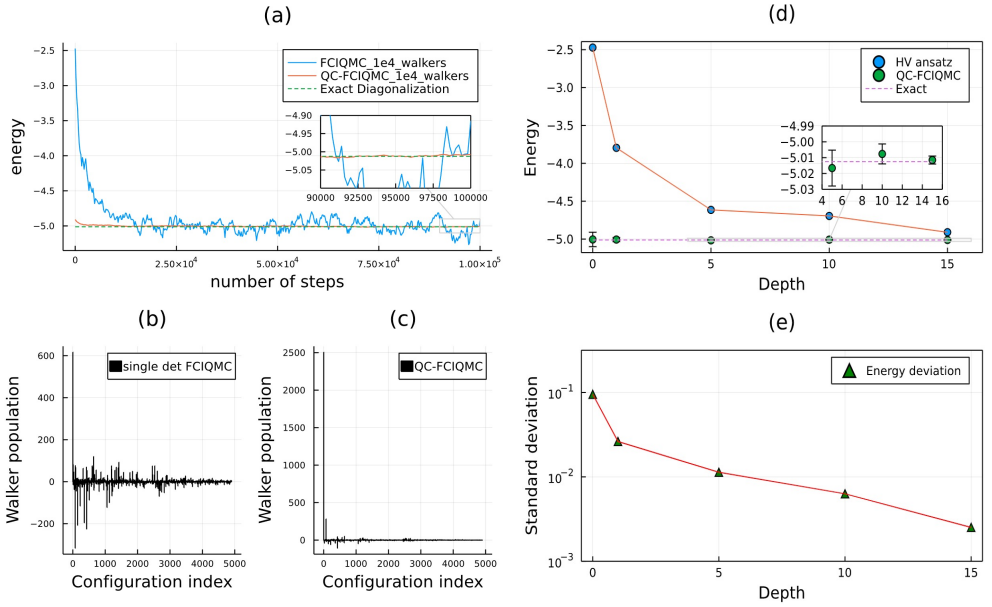


Figure 6. Comparison of the classical FCIQMC and QC-FCIQMC with basis generated by the Hamiltonian variational (HV) ansatz on the  $2 \times 4$  Hubbard model ( $U/t = 4$ ). The HV ansatz with 1, 5, 10, 15 layers is implemented for comparison of variance suppression. The energy shift starts at  $10^4$  walkers for all cases. (a) Comparison of energy fluctuation for FCIQMC and QC-FCIQMC. (b) Walker population for single determinant FCIQMC. (c) Walker population for QC-FCIQMC. (d) Energy estimation for different setups of layer number. (e) Effect of variance suppression.